ISTITUTO NAZIONALE DI RICERCA METROLOGICA
Repository Istituzionale

High-performing vapor-cell frequency standards

(Article begins on next page)

06 September 2024

High-performing vapor cell frequency standards

A. Godone(1), F. Levi(1), C. E. Calosso(1) and S. Micalizio(1)(*)

(1) INRIM, Istituto Nazionale di Ricerca Metrologica - Torino, Italy

Summary. — Many nowadays scientific and technological applications need very precise time and frequency reference signals. Very often, only atomic clocks can guarantee the high level of accuracy and stability required by these signals. In the current scenario of atomic frequency standards, vapor-cell clocks are particularly suited to be employed in those activities that demand for good frequency stability performances joined to compactness, reliability and low power consumption. Recently, due to better performing laser sources and to innovative techniques to prepare and detect the atoms, several cell-based prototypes exhibiting unprecedented frequency stability have been developed.

We review advances in the field of laser pumped vapor-cell clocks and we provide an overview of the techniques that allowed to achieve frequency stabilities in the order of 1×10^{-13} at 1 s (short term) and in the range of 10^{-15} for the medium-long term. These stabilities are two orders of magnitude better than current commercial Rb clocks.

We also prospect the possibility of further improving these results.

PACS 06.30.Ft – Time and frequency.
PACS 32.70.Jz – Line shapes, widths, and shifts.
PACS 32.30.Bv – Radio-frequency, microwave, and infrared spectra.
PACS 32.80.Xx – Level crossing and optical pumping.

1. – Introduction

Since their first realization in the 1960's, lamp-pumped Rb clocks have been used as precise frequency and time references because of their good short-term frequency stability performances [1, 2, 3, 4]. Depending on the manufacturer, commercial implementations of gas-cell Rb clocks exhibit a frequency stability, in terms of Allan deviation, in the range 0.5 to 1×10^{-11} for 1s of integration time.

Thanks to the additional properties of being compact and relatively inexpensive, Rb clocks are adopted where the requirements regarding frequency stability cannot be satisfied by quartz oscillators and where, at the same time, constraints on size, power

(*) Email: s.micalizio@inrim.it

consumption or cost prevent the use of other frequency standards. Every year, several thousands of Rb clocks units are sold, and they are exploited in a number of technological fields, including laboratory equipment as well as space applications, such as the satellite navigation systems GPS [5], GALILEO [6], GLONASS [7], and COMPASS [8].

The development of single mode semiconductor laser diodes in the 1980's opened new interesting prospects in the field of gas cell frequency standards, thanks to the possibility of replacing the discharge lamp with a laser source resonant on D_1 or D_2 spectral lines of alkali-metal atoms.

First, a much simpler system without the need of the hyperfine filter could be implemented, reducing at the same time size and power consumption. Later, the laser coherence properties enabled the investigation of peculiar interrogation schemes, like coherent population trapping, absolutely unfeasible in a lamp-pumped device.

The main advantage relies, however, in the fact that the laser spectrum is much narrower (< 100 MHz) than that of a lamp (≈ 1 GHz), resulting in a more efficient optical pumping. Accordingly, hyperfine resonance lines with contrasts of the order of 10% or even higher have been predicted and observed.

There are two main trends in the current research on laser pumped vapor cell clocks. The first is the extreme miniaturization which aims at realizing a vapor-cell atomic clock as small as a cm^3. If, on one hand, this miniaturization process has many advantages (e.g. power consumption of a few tens of mW, reduced mass and production cost), on the other hand the short-term stability is necessarily limited to units of 10^{-10} (at 1s) by the size of the microfabricated cell and then by the number of interacting alkali-metal atoms. Miniaturized atomic clocks are developed in view of future applications in mobile and low-power instrumentation or hand-held devices (see for example [9, 10, 11, 12, 13, 14, 15]).

The other research activity consists of pushing the vapor cell clocks stability performances to the limit: compared to a lamp-pumped approach, the expected improvement is in effect theoretically estimated 2-3 orders of magnitude, predicting a white frequency noise limit at the level of 1×10^{-14} for a measurement time of 1s [16].

In fact, compared to a lamp-pumped device, only one order of magnitude has been experimentally gained in the short-term frequency stability. The reason is that the previous estimate refers to the shot-noise associated to the detected photons, but other noise sources overcome this ultimate limit in a laser-pumped gas cell clock. In particular, we will see that the laser frequency noise as well as the microwave phase noise transferred to the clock signal do not allow to reach the expected theoretical limit. Indeed, the attempt of approaching the ultimate shot-noise limit is supported by the always increasing demand of highly stable local oscillators and for this purpose in the past twenty years new schemes have been considered.

These techniques include laser noise compensation in a continuously operated clock, coherent population trapping (CPT) and pulsed optical pumping (POP) in a Ramsey scheme. Adopting these techniques, frequency stabilities, in terms of Allan deviation, as low as $\sigma_y(\tau) \approx 10^{-13}\tau^{-1/2}$ (τ being the measurement time) have been achieved [17] and, in some cases, the white frequency noise region extended up to 10^4 s, reaching a stability at the level of units of 10^{-15} [18].

Evidently, engineered implementations of these devices would be competitive not only compared with lamp-pumped Rb clocks currently used in many advanced fields, such as space, but also compared with passive H-masers (PHM). For example, an optimized prototype of the POP clock is expected to have a volume less than 15 liters, a mass of 9 kg and a power consumption less than 40 W; these values are approximately a factor of two lesser than those of the GALILEO PHM [19]. At the same time, the engineered

POP clock would maintain the good properties of a lamp-pumped Rb clock, such as a simple physics package and implementation costs relatively low, and would have a frequency stability comparable or even better that that of a PHM. On the other hand, the reliability of the laser source is an issue. However, we do not tackle in this work the topic of the technological development of laser-pumped cell clocks. The interested reader can refer to the literature (see for example [20, 21])

Rather, in this paper we provide a review of physical and metrological aspects of high-performing vapor cell clocks developed by various research groups. We will describe the proposed techniques outlining their main advantages and limitations and the most significant results. In particular, we limit this review to the works in literature where a clock stability measurement has been reported.

Chapter 2 reminds the basic interactions taking place in a laser-pumped cell. In the following chapters we describe the approaches that recently led to the achievement of short-term frequency stabilities at the level of units of 10^{-13} at 1 s. These include the continuous-wave double resonance (DR) approach (chapter 3), the CPT standards operating both in the continuous and in the pulsed modes (chapter 4) and the intensity optical pumping scheme in the pulsed mode (chapter 5). In chapter 6, very recent proposals will be analyzed concerning the reduction of the laser noise contributions in the detection phase and the reduction of the microwave phase noise transferred to the atoms by aliasing effect. The phenomena affecting the long-term stability will be considered in chapter 7. Finally, in chapter 8 we will also examine the implementation of a cell clock using a cold sample of atoms.

2. – Basic interactions in the cell

In this chapter we briefly remind the interactions the atoms undergo in typical vapor-cell experimental arrangements realized for frequency standards purposes. Except for the case in which the CPT resonance is detected in the optical domain (see later), in all the other cases the setup includes an alkali-metal vapor cell and a microwave cavity. The vapor cell contains Rb or Cs and a buffer gas and is placed in the microwave cavity resonating at the (angular) frequency ω_C close to the ground-state splitting. The cavity is characterized by a loaded quality factor Q_L and by a detuning $\Delta\omega_C \equiv \omega_C - \omega_{\mu\mu'}$ with respect to the atomic resonance frequency $\omega_{\mu\mu'}$. The buffer gas is added to the cell to inhibit Doppler broadening of the hyperfine clock transition and to reduce the relaxation on the cell walls (Dicke narrowing [22]). Nitrogen is generally used as buffer gas since it quenches the fluorescence radiation in an optically thick Rb vapor. Fluorescence quenching prevents radiation trapping which would decrease the effectiveness of the optical pumping [4].

In addition, the atoms are supposed to interact with either one or two phase-coherent laser beams connecting the ground states to an excited state; the latter case corresponds to the so called Λ scheme responsible of the CPT phenomenon. Basic parameters to describe the interaction with the electromagnetic fields are the Rabi frequencies associated to the externally applied microwave and to the laser field; in the following we will refer to them as b_e and ω_R respectively (ω_{R1} and ω_{R2} for the Λ scheme). These quantities are proportional to the respective fields amplitudes.

Moreover, an internal RF field coupling the two ground-state hyperfine levels is present in the cavity. This field is created by the atomic ensemble itself due to the cavity feedback on the atomic sample [23].

The physics package is in general completed by a quantization static magnetic field

$\mathbf{B}_0$, a set of magnetic shields and a heater to operate the clock at the desired temperature. In particular, $\mathbf{B}_0$ is applied to the atoms in order to remove the Zeeman degeneracy in the ground-state and is considered as a static-perturbation. Owing to selection rules for dipole transitions, in most of practical realizations laser propagation direction, microwave field and quantization magnetic field are collinear.

We have also to consider relaxation and excitation not induced by coherent fields. In particular, buffer gas and spin-exchange collisions are sources of relaxation in the ground-state. Specifically, we call γ_1 the (longitudinal) relaxation rate for the ground-state population and γ_2 the (transversal) relaxation rate for the ground state coherence. Explicit forms of the various relaxation terms can be found in [4]. We only remind that for typical buffer gas pressures, operation temperatures and cell sizes, γ_1 and γ_2 are of the same order of magnitude and are in the range $200 \div 1000$ s^{-1}.

Buffer gas not only affects the ground state but also the excited state. Specifically, it causes homogeneous broadening and red-shift of the optical line. For a buffer gas pressure of 25 Torr the optical line is of the order of 1 GHz, much larger than the spontaneous emission broadening (5 MHz) and also larger than Doppler broadening (≈ 500 MHz), while the red-shift is of the order of 150-180 MHz. We characterize the excited state broadening by a relaxation rate Γ^* that is about $2-5 \times 10^9$ s^{-1} at the pressures commonly used in frequency standards.

It is then useful to introduce the laser pumping rate defined as:

$$(1) \qquad\qquad \Gamma_p = \frac{\omega_R^2}{2\Gamma^*}$$

that in frequency standards applications ranges in the interval $(10^3 \div 10^5)$ s^{-1}.

The atoms are considered as three-level systems (the two ground state levels and an exited state) and their evolution is conveniently analyzed in the density matrix $\hat{\rho}$ formalism where the diagonal elements ρ_{ii} take into account the dynamical evolution of the atomic levels populations and the elements ρ_{ij} $(i \neq j)$ refer to the coherences excited among them by the coherent fields. For an optically thick medium, absorption of the laser field as it propagates in the atomic medium must be taken into account. In this case, it is possible to write the Maxwell-Bloch equations for a three-level system under microwave and optical excitation, either in a DR approach or in a Λ scheme and they have been used to derive all the results reported in the following sections. These equations can be explicitly found in [24] or [25].

The analysis can be extended to a multi-level system to include the Zeeman structure, as done for example in [26].

We mention that in a different approach, the cell does not contain any buffer gas but is paraffin-coated. The interest for wall coated cells relies in the possibility of achieving very small relaxation rates (see for example [27, 28]). Recently, a rubidium atomic frequency standard based on a paraffin-coated cell has been realized, exhibiting a short-term frequency stability of about $3 \times 10^{-12}\tau^{-1/2}$ between 1 and 100 s [29], not yet at the level of high-performing clocks adopting buffer gas cells.

3. – The continuous-wave (CW) double-resonance Rb clock with laser optical pumping

In this approach, a laser diode tuned to either D$_1$ or D$_2$ optical transition of ^{87}Rb replaces the lamp as a source of optical pumping. The scheme of principle of the setup is

shown in Fig. 1, whereas the scheme of the levels involved in the interaction is reported in Fig. 2.
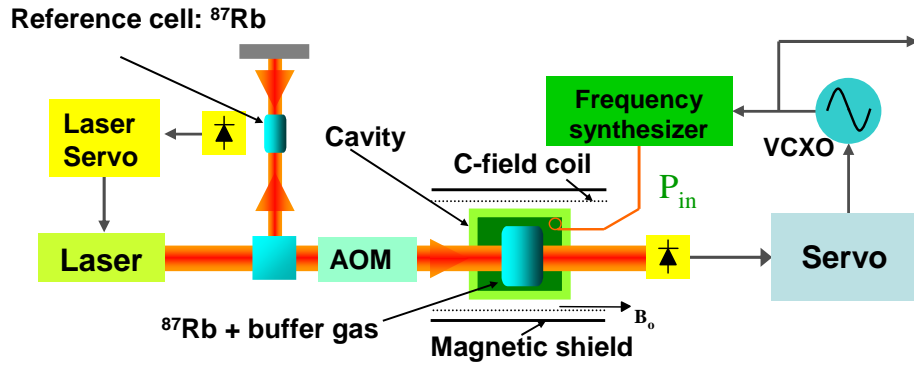

Fig. 1. – Schematic of a laser-pumped Rb clock in the configuration exploiting an AOM; VCXO: Voltage Controlled Crystal Oscillator.
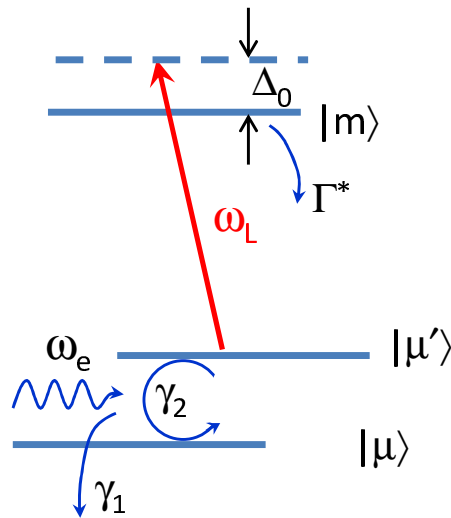

Fig. 2. – Three-level scheme considered for the continuous DR Rb clock; $\Delta_0/2\pi$ is the laser detuning with respect to the optical transition; ω_L is the laser angular frequency and ω_e is the (angular) frequency of the externally applied microwave.

In the most diffused setups, the laser is frequency locked to the optical line using an external cell containing only ^{87}Rb by the common sub-Doppler saturated absorption technique [30]. Due to the red shift of the optical resonance produced by the buffer gas, an acousto-optic modulator (AOM) may be used to move the laser frequency so that it matches the optical transition frequency in the clock cell. We note, however, that in some experimental configurations, light-shift was considerably reduced despite

the red shift and without using an AOM (see the discussion about intensity light-shift suppression at p. 8).

Similarly to a lamp-pumped device, the laser light depletes one of the two ground state levels populating the other one through optical pumping. Simultaneously, a microwave field resonating with the ^{87}Rb clock transition is applied to the atoms. The light power transmitted through the cell versus the applied microwave frequency carries the clock signal used to correct the frequency of the microwave local oscillator Fig 1. The signal is well described by a Lorentzian shape whose full width at half maximum (FWHM) $\Delta\nu_{1/2}$ can be written as [25]:

$$(2) \qquad\qquad \Delta\nu_{1/2} = \frac{1}{\pi}\sqrt{b_e^2 + (\gamma_2 + \Gamma_p)^2}$$

where the laser ($\propto \Gamma_p$) and microwave ($\propto b_e$) broadenings are clearly evident.

This approach has been extensively studied in the past from different points of view. One interesting aspect has been the investigation of new physical phenomena, especially those related to the laser-atom interaction, like light-shift. On the other hand, the perspective of developing a new type of atomic clock has considerably intrigued the frequency metrology community. However, despite the prediction of great improvement in frequency stability performances [16], it has been soon realized that the cell is a very complex device in which microwave and optical signals influence each other in non trivial way, significantly affecting in the end the clock stability.

Different research groups using a variety of laser sources investigated the continuous laser optical pumping technique in a Rb frequency standard (see for example in the Vanier's paper [25]). Here we recall the most recent and performing results.

Among the several notable achievements, we remind that of Saburi et al. [31] who obtained a frequency stability of $1 \times 10^{-12}\tau^{-1/2}$ ($1 \leq \tau \leq 200$ s) with a DBR laser having a spectral width of 500 kHz. Camparo et al. [32] used a junction transverse stripe laser (JTS) with a line width of 21 MHz and the measured clock's frequency stability was $1.8 \times 10^{-12}\tau^{-1/2}$ (for $1 \leq \tau \leq 10$ s). The interesting aspect of this work is that the laser is frequency locked on the same cell used for clock purposes, realizing a very compact device. A frequency stability of $3 \times 10^{-13}\tau^{-1/2}$ ($1 \leq \tau \leq 20$ s) is reported by Mileti et al. [33] with a 3 MHz linewidth DBR laser. Particular attention was adopted in this work to reduce the microwave noise transferred to the clock signal through the inter-modulation effect [34]. The achieved short term frequency stability has been for about ten years the best result obtained for a laser pumped DR system.

A very interesting solution has been adopted in [35] to reduce the impact of laser frequency modulation (FM) to amplitude modulation (AM) noise conversion on the clock's short term frequency stability. The clock uses two identical physics packages so that a clone cell, not involved in the microwave interaction, is used to create an intensity noise correlated to that of the clock cell. A noise subtraction technique allows to significantly improve the short-term stability from $1.1 \times 10^{-12}\tau^{-1/2}$, when only one cell is used, to $5.3 \times 10^{-13}\tau^{-1/2}$, when laser FM-AM noise subtraction is active. The medium-long term stability of this clock reaches 3×10^{-14} at $\tau \approx 300$ s.

In a more recent work, a high-performance laser-pumped Rb clock was demonstrated [36, 37]. This clock uses a Rb cell placed in compact magnetron-type cavity [38]. Thanks to the electrodes arrangement, this cavity resonates on the electromagnetic TE$_{011}$-like mode in a smaller volume compared to a traditional cylindrical resonator, the reduction

factor being of the order of 3. The complete physics package includes heater and magnetic shields, with a total volume < 1 liters and mass ≈ 1.4 kg. The clock has then a compact volume, reduced mass and low power consumption, similar to those of conventional lamp-pumped devices.

The remaining setup is composed of a laser system based on a DFB diode emitting at 780 nm (D_2 transition for ^{87}Rb) and a dedicated low-phase noise electronics [39] which guarantees a contribution to the clock stability via the inter-modulation effect at the level of 7×10^{-14} at 1 s.

The observed clock resonance is a Lorentzian with a linewidth of 361 Hz (FWHM) and a signal contrast of 26 %.

The measured clock stability turns out as low as $1.4 \times 10^{-13} \ \tau^{-1/2}$ for integration times τ up to 100 s. For longer τ, the stability is limited by a flicker floor. A noise budget analysis shows that the short-term stability is affected by FM-to-AM conversion of laser FM noise. This process significantly degrades the shot-noise limit that for this clock is expected to be $\approx 5 \times 10^{-14} \ \tau^{-1/2}$. The long-term stability is instead related to light-shift, specifically to its resonant component (FM-FM conversion). Therefore, laser instabilities result to affect both the short and the long term performances of continuous DR Rb clocks and in the following subsections we will quickly describe the physical mechanisms through which laser fluctuations are transferred to the atomic clock transition.

We conclude this section by reminding that the CW double resonance scheme can be operated in the maser configuration. In this case, the Rb cell is placed in a high-Q cavity ($Q \approx 30000$) and similarly to an active H-maser, a self-sustained oscillation is observed between the two clock levels [40, 41]. Several studies were done in the past using either a lamp or a laser as source of the optical field. For laser pumped Rb masers, studies were mainly focused into the physical characterization of the prototypes [42], including light-shift [43] and the Q-enhancement technique [44], but not significant results in terms of frequency stability were reported.

For lamp-pumped Rb masers, some frequency stability measurements are reported [45, 46, 47] and in the best cases, values of units of 10^{-13} was achieved [48, 49]. However, the long term is dominated by thermal fluctuations through the cavity pulling effect and a frequency stability below the 10^{-13} level was never observed.

3˙1. *Light-shift*. – When a nearly resonant optical field interacts with an atom, atomic energy levels are shifted by the so called AC Stark shift [50, 51]. The two levels involved in the interaction shift of the same amount but in opposite directions (see Fig. 3).

The light-shift $\Delta\omega_{LS}$ of the clock transition can be written as:

$$(3) \qquad \Delta\omega_{LS} = \frac{\omega_R^2}{4} \frac{\Delta_0}{(\Gamma^*/2)^2 + \Delta_0^2}$$

It is then proportional to the laser intensity I_L through the optical Rabi frequency ($I_L \propto \omega_R^2$) and versus the optical detuning is a lorentzian dispersive curve.

In the continuous operation mode, light-shift is conveniently characterized in terms of two parameters strictly related to experimental situations: a) the frequency light-shift coefficient β_{LS} that for a given laser intensity gives the slope of the dispersion pattern;

b) the intensity light-shift coefficient α_{LS} related to the fact that, for a given laser detuning, $\Delta\omega_{LS}$ is proportional to the laser intensity. Actually, $\Delta\omega_{LS}$ is not exactly linear with laser intensity due to inhomogeneity in the laser excitation; therefore, it is
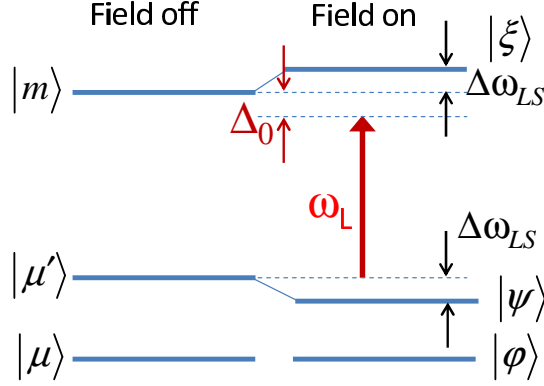
Fig. 3. – Light shift in a two-level system.

more appropriate to renormalize α_{LS} to the fractional change of laser intensity, defining $\alpha_{LS\%} = \alpha_{LS}/(\Delta I_L/I_L)$.

Typical values of these coefficients are reported in Table 1 of chapter 5.

They are relatively large and light-shift is recognized as one of the main source of instability in the medium long term.

Some techniques can be envisaged to reduce light-shift. Equation (3) simply states that $\Delta\omega_{LS}$ scales as Γ^{*2}: a high-buffer gas pressure can be used to broaden the optical line in the resonance cell [32, 52]. However, in this case also the ground-state relaxation rates increase, with a consequent broadening of the clock resonance linewidth.

In another approach, it is possible to lock the laser frequency to a particular sub-Doppler transition that minimizes $\alpha_{LS\%}$, as done for example in [53, 54]. Moreover, it is possible to reduce the influence of β_{LS} by lowering the laser intensity at the cell entrance.

We will see that CPT, using two-phase coherent lasers, provides a first-order cancellation of light-shift, whereas in the POP technique light-shift remains only at a residual level.

3˙2. *Short-term frequency stability*. – We have seen that laser instabilities affect both the short and the medium long term clock performances. The purpose of this section is to give a more precise picture of the main phenomena contributing to limit the short-term frequency stability.

The variance $\sigma_y^2(\tau)$ of the clock signal can be written as:

$$(4) \qquad \sigma_{y,tot}^2(\tau) = \sigma_{y,sh}^2(\tau) + \sigma_{y,RIN}^2(\tau) + \sigma_{y,FM-AM}^2(\tau) + \sigma_{y,LO}^2(\tau)$$

In Eq. (4), the first term is the fundamental shot noise contribution that, as we have seen, is expected at the level of 10^{-14}. However, besides the shot noise term, the clock variance receives other contributions.

The second term is related to the laser relative intensity noise (RIN) which modulates the laser amplitude at the laser output. This noise is transmitted through the cell and is detected by the photodiode as noise directly added to the shot noise component (AM-AM). To give an estimate of its contribution to frequency stability, we refer for example

to [55] where for a DFB laser a $RIN(f) \approx 2 \times 10^{-14}$/Hz at 300 Hz has been measured and the contribution to the clock stability results $\sigma_{y,RIN}(\tau) \approx 10^{-14} \ \tau^{-1/2}$.

The third term is the already mentioned FM to AM conversion [56, 57, 58]. To shortly review the physical mechanisms at the basis of this effect, we consider the well know Lambert-Beer law describing the exponential attenuation of a laser beam of intensity I_{0L} propagating through a medium of given susceptibility $\chi = \chi' + i\chi''$:

$$(5) \qquad\qquad I_L(z) = I_{0L} \exp\left(-\alpha \int_0^z \chi''(z')dz'\right)$$

where the imaginary part of the susceptibility is responsible of the attenuation (α is the absorption parameter). It is easy to show that, in terms of atomic variables, χ'' is proportional to the optical coherence excited by the laser. Therefore, the laser phase instabilities induce fluctuation in the coherences and consequently stochastic variation in χ'' and then in the optical attenuation. The absorbing medium then converts FM fluctuations of the laser into AM intensity fluctuations. It is a non-linear phenomenon whose efficiency depends on the laser linewdith (indeed, the linewidth is proportional to the variance of phase fluctuations) and on the thickness of the medium . If we make an estimate of its contribution to the frequency stability we find a value of the order of $\sigma_{y,FM-AM}(\tau) \approx (1 \div 3) \times 10^{-13} \ \tau^{-1/2}$.

The last term in Eq. (4) is responsible of another effect limiting in dramatic way the short term frequency stability of all passive clocks: the microwave inter-modulation effect. Noise spectral components around even harmonics of the modulation frequency are filtered by the atoms and down-converted by aliasing to low frequency noise (Dick effect for pulsed clocks). State of the art of low-phase noise synthesis chains guarantees a contribution to the clock's stability at the level of $\sigma_{y,LO}(\tau) \approx (7 \div 10) \times 10^{-14} \ \tau^{-1/2}$.

Indeed, the last two effects represent the two technical noises limiting the short-term stability performances of all current prototypes of vapor cell clocks, operating both in the continuous and in the pulsed modes. Reducing them is really a challenging task which involves different research groups. We will see in chapter 6 some proposals to overcome them, allowing, as a consequence, to approach the shot-noise limit.

4. – CPT based standards

In previous section, the laser is mostly used because of its narrow spectrum, rather than for its coherence. Instead, an important phenomenon in which the coherence properties are fully exploited is CPT. CPT is a very well investigated phenomenon, the literature on this topic is very vast, concerning both physics (see for example [59]) and frequency metrology studies (see [60] and [61]). Here we will remind the basic principle and we will give an overview of the main results in vapor cell clocks applications.

CPT was observed for the first time in a Na cell using a multimode dye laser [62]. A longitudinal gradient of magnetic field was also applied to the cell and the fluorescence was observed as a function of the position in the cell. At longitudinal locations where the ground-states hyperfine frequency matched the frequency difference between two laser modes, dark lines were observed in the fluorescence, as shown in Fig. 4.

After the discovery of these resonances and their explanation through the coherent population trapping mechanism, these narrow features were recognized as possible microwave frequency references, first in an atomic beam [63, 64, 65] and later in a gas cell

Fig. 4. – First observation of a dark line in a Na cell. Courtesy of E. Arimondo.

[66]. Since then, the study of CPT application to clocks considerably increased and has been carried on by several research groups still today.

4˙1. *The phenomenon*. – The CPT phenomenon is easily observed in alkali-metal atoms when the two ground-state $^2S_{1/2}$ hyperfine levels are coupled to the P state via two phase-coherent laser radiations (Λ scheme), as shown in Fig. 5.

At resonance, that is when the laser frequency difference equals the ground state hyperfine splitting, the atoms no longer absorb energy from the laser light, the scattered radiation is greatly reduced and a dark line appears in the fluorescence spectrum. The dark line or the equivalent electromagnetically induced transparency (EIT) line observed in the transmission spectrum can be used as reference clock signals.

These CPT hyperfine resonances are generated without any microwave cavity since the bichromatic laser field itself carries the microwave needed by the atoms to excite the hyperfine transition. This allows the realization of very compact clocks, reducing at the same time the detrimental effects related to the cavity (e.g. cavity pulling).

We notice that, interestingly, CPT generates a strong coherence coupling the two ground-state hyperfine levels. This coherence is the source of an oscillating magnetization leading to the emission of coherent microwave radiation [67]. This emission can be observed when the atomic sample is placed in a microwave cavity tuned to the oscillating magnetization frequency (CPT maser). The CPT maser as well can provide a stable frequency signal useful for the implementation of a vapor cell clock.

4˙2. *Dark lines and CPT maser*. – Figures 6 and 7 show schematics of the setups used to detect CPT transitions both in the optical and in the microwave domain.

The laser radiations can be provided in different ways: 1) by the first side-bands of a phase modulated laser; 2) by two independent offset-locked lasers or 3) by modulating
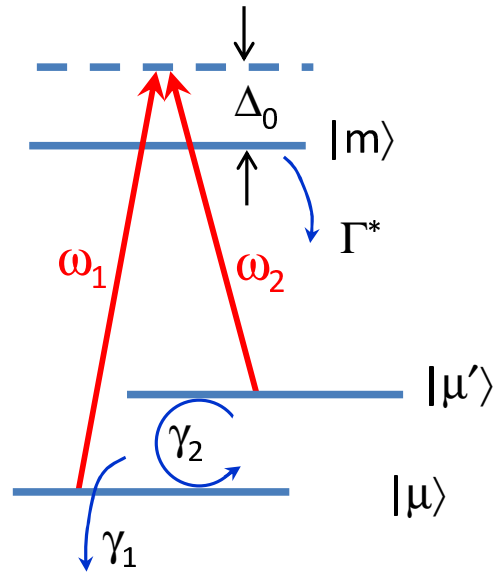
Fig. 5. – Three-level system under Λ scheme; ω_1 and ω_2 are the laser angular frequencies.
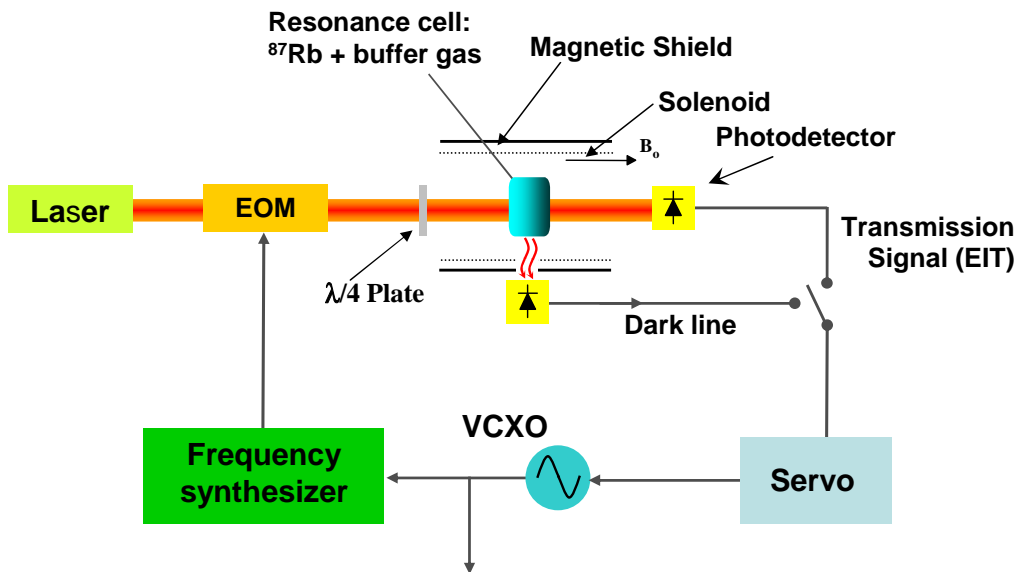

Fig. 6. – Schematic setup of the CPT clock based on the dark line or on the EIT signals. EOM: Electro-optic modulator. VCXO: Voltage Controlled Crystal Oscillator. Laser stabilization and thermal controls not shown in the figure.

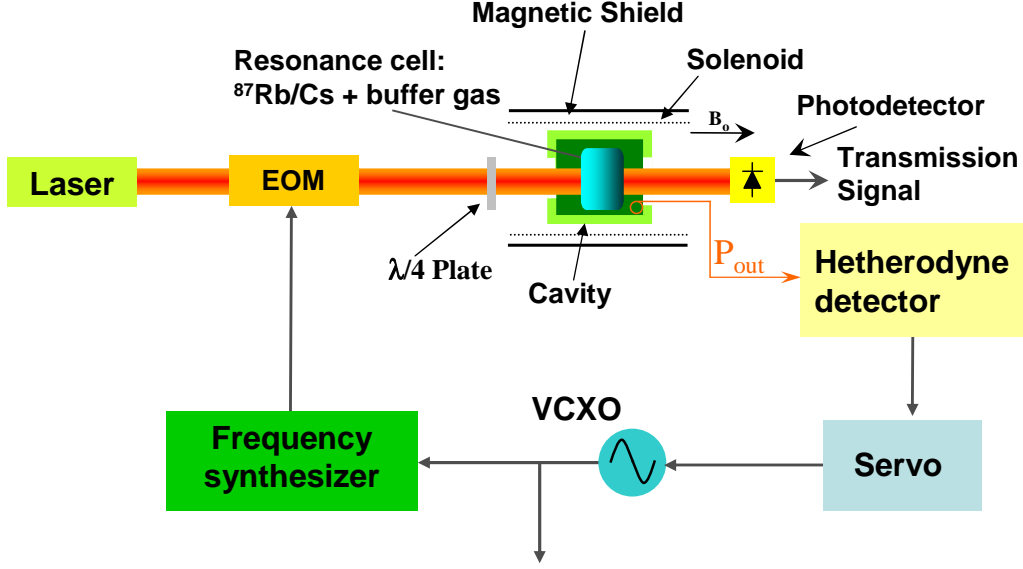directly the injection laser current. However, the first technique is preferable compared

Fig. 7. – Schematic setup of the CPT maser.

to the other two in terms of compactness of the setup and symmetry properties of the output laser spectrum. In this case in effect, the setup includes an electro-optic phase modulator (EOM) driven by a RF synthesizer. The modulation index m_ϕ is related to the power injected by the synthesizer into the EOM.

The polarization conditions for the laser fields to generate the Λ scheme are discussed for example in [68].

The atomic system can be analyzed in the ensemble-averaged density matrix $\hat{\rho}$ formalism recalled in chapter 2. We first consider the case of a thin, homogeneous, three-level atomic sample ($\zeta \ll 1$) in the long wavelength ($L \ll \lambda_{\mu w}$) approximation, $\zeta = \frac{\alpha L}{\Gamma^*}$ being the optical length of the sample, α the absorption parameter [69], L the cell length and $\lambda_{\mu w}$ the wavelength of the hyperfine transition.

The dark line and the EIT signals are both proportional to the matrix element ρ_{mm} (excited state population) that in this approximation and for $\omega_{R1} = \omega_{R2}$ is given by [67, 68]:

$$(6) \qquad \rho_{mm} = \left(\frac{\omega_R}{\Gamma^*}\right)^2 \left[1 - \frac{2\Gamma_p (\gamma_2 + 2\Gamma_p)}{(\gamma_2 + 2\Gamma_p)^2 + \Omega_\mu^2}\right]$$

where $\Omega_\mu \equiv (\omega_1 - \omega_2) - \omega_{\mu\mu'}$ is the two-photon Raman detuning.

Figure 8 shows the dark line (a) and the EIT (b) signals observed in a ^{87}Rb cell containing also a mixture of Ar and N$_2$ as buffer gas. The resonances have been observed in a low temperature (30 ^{O}C) and low optical pumping rates regime, ($I_L \approx 200 \; \mu W/cm^2$ for each sideband, corresponding to a pumping rate $\Gamma_p \approx \gamma_2 \approx 300 \; s^{-1}$ at this temperature).

In the case of the CPT maser approach, the power emission profile P_a of the atomic
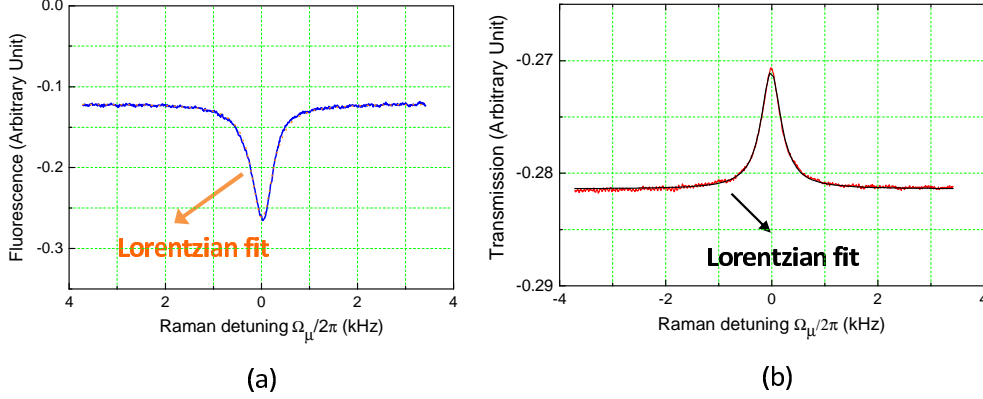
Fig. 8. – Dark line (a) and transmission spectrum (a) versus two-photon Raman detuning. The cell was 5 cm long and the laser was tuned on D_2 transition.

ensemble is proportional to the square of the coherence excited in the ground-state by the CPT phenomenon and can be written as [67]:

$$(7) \qquad P_a = \frac{1}{2}\hbar\omega_{\mu\mu'} N_a k \frac{(2\Gamma_p)^2}{(\gamma_2 + 2\Gamma_p)^2 + \Omega_\mu^2}$$

N_a being the number of atoms in the volume of the cell exposed to the radiation fields and $k = \frac{\mu_0 \mu_B^2 \eta' Q_L n}{\hbar}$ the number of microwave photons emitted by an atom in 1s (μ_0 is the free space permeability, μ_B the Bohr magneton, Q_L the loaded cavity quality factor, η' the filling factor and n the atomic density). The maser emission at $\omega_1 - \omega_2$ and the absence of an oscillation threshold [23] are features similar to those observed in the case of passive masers.

In Fig. 9 we report on a typical CPT maser emission profile. The figure refers to a 18 mm long cell with ^{87}Rb and 25 Torr of Ar and N_2 as buffer gas.

As far as the approximation of a thin and homogeneous medium is valid, in both the optical and the microwave detection modes, the clock reference lineshapes are Lorentzian with a full-width at half maximum (FWHM) given by:

$$(8) \qquad \Delta\nu_{1/2} = \frac{1}{\pi}\left(\gamma_2 + 2\Gamma_p\right)$$

Equation (8) simply states that, as in the case of CW DR laser-pumped clocks, the linewidth broadens with the laser intensity (power broadening). It is important to point out that in the CPT maser approach the clock signal is observed in absence of any background, whereas in the dark line or EIT ones the resonances are superimposed to a significant background level of light signal.

In practical operating conditions, the CPT maser output power is of the order of 10 pW; the FWHM is in the range $\Delta\nu_{1/2} \approx 150 \div 250$ Hz and the EIT contrast $C \approx 5 \div 20\%$.
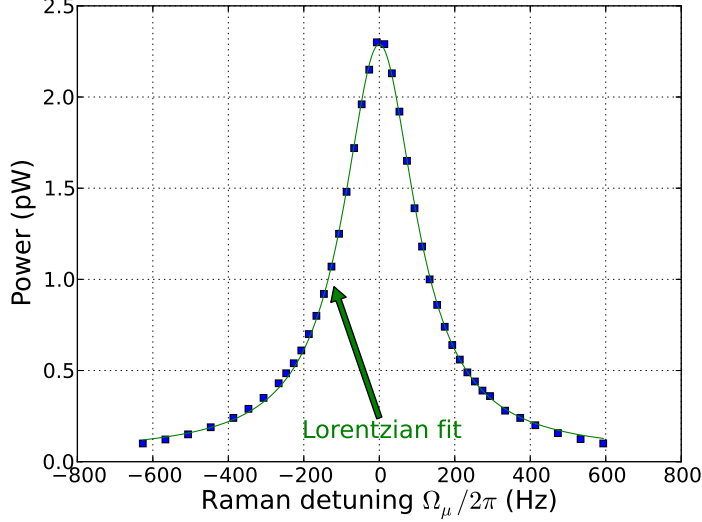
Fig. 9. – Emission profile of the CPT maser. Cell temperature 68 $^{\rm O}$C; $\Gamma_p = 500$ s^{-1}.

For the Λ excitation scheme of Fig. 5 the **resonant light-shift** $\Delta\omega_{LS}$ is found to be [67]:

$$(9) \qquad \Delta\omega_{LS} = -\frac{1}{4}\left(\omega_{R1}^2 - \omega_{R2}^2\right)\frac{\Delta_0}{(\Gamma^*/2)^2 + \Delta_0^2}$$

When $\omega_{R1} = \omega_{R2}$ the excitation scheme is highly symmetric, no population difference occurs in the ground-state hyperfine levels and $\Delta\omega_{LS} = 0$: indeed, this property has been one of the main reasons to develop frequency standards based on the CPT phenomenon (no FM-FM conversion). From a physical point of view, we can interpret this light-shift cancellation as a consequence of the fact that the dark state does not interact with the light and then does not experience any Stark shift.

A deeper analysis of light-shift considers the effect of each laser field on the other transition of the Λ scheme, as well as any non resonant component possibly present in the laser spectrum. Even if off-resonant (no real transitions are induced), these components create a perturbation of the system and are sources of light-shift (**off-resonant light-shift**).

In the case of a phase modulated laser it has been found [70, 71]:

$$(10) \qquad \frac{\Delta\omega_{LS}}{\omega_{\mu\mu'}} = \left(\frac{\omega_{RL}}{\omega_{\mu\mu'}}\right)^2\left[\Theta(m_\phi) + \Xi(m_\phi)\left(\frac{\Delta_0}{\omega_{\mu\mu'}}\right)^2\right]$$

where ω_{RL} is the angular Rabi frequency of the unmodulated laser and m_ϕ the modulation index. The analytical expressions of $\Theta(m_\phi)$ and $\Xi(m_\phi)$ are reported in [70] and

their behavior is sketched in Fig. 10; both these coefficients have zeroes as function of m_ϕ. The first term, proportional to $\Theta(m_\phi)$ is responsible of a pure power light-shift contribution (AM-FM conversion) which can be minimized for $m_\phi = 2.4$ where $\Theta(m_\phi)$ is approximately zero. In practical applications, however, this term makes hard to reduce the clock frequency stability below the 10^{-13} level in the medium term: temperature fluctuations affect the EOM operation, so that it is hard to keep stable in time the value of the modulation index which makes light shift negligible. The second term, proportional to $\Xi(m_\phi)$ is responsible of a quadratic light-shift contribution and may be neglected in real operating conditions.
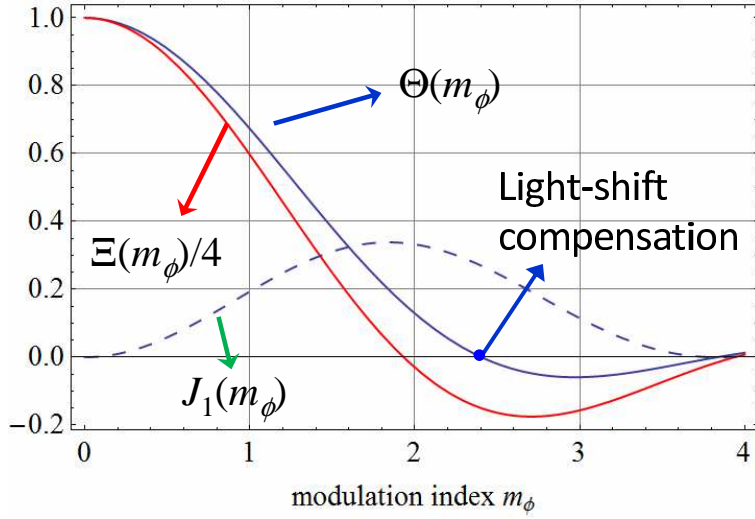

Fig. 10. – Behavior of the functions of Eq. (10) versus the modulation index of the microwave signal driving the EOM. A comparison is done with the Bessel function $J_1(m_\phi)$ which gives the amplitude of the first modulation sidebands.

For a description of CPT frequency standards in a manner closer to practical operating conditions, we have to remove the hypothesis done so far. Typically the atomic sample is not thin, the long wavelength approximation does not hold and the multiplicity of levels can limit the excitation of the dark states. In this case, new effects appear that influence the resonance lineshape and/or the standard stability.

In the CPT maser, the feedback parameter k increases with the atomic density and the cavity quality factor. When k becomes comparable to γ_2 the microwave cavity feedback on the atomic ensemble cannot be neglected [23]. In this condition, the pure resonant light-shift is still negligible when $\omega_{R1} = \omega_{R2}$ as predicted by Eq. (9), but a **microwave shift** $\Delta\omega_{MS}$ appears. This shift induces an imbalance in the ground state populations even when $\omega_{R1} = \omega_{R2}$ and leads to a residual optical pumping that shifts the emission profile [69, 72]:

(11)
$$\Delta\omega_{MS} = K_{MS}\Delta_0 \text{ for } \Delta_0 \ll \Gamma^*/2$$

where K_{MS} is an increasing function of both k and ω_R. In typical operating conditions

this FM-FM conversion factor turns out $K_{MS} \approx 1 \times 10^{-12}$/MHz [72].

The cavity feedback on the atomic medium is also responsible of a **cavity pulling shift** $\Delta\omega_{CP}$. For a thick medium ($\zeta > 1$) no analytical solution is available for $\Delta\omega_{CP}$, but its physical behavior can be described by the following relation, valid for a thin medium [23, 72]:

$$(12) \qquad \Delta\omega_{CP} = \frac{Q_L}{Q_a} \frac{k^2 |2\delta_{\mu\mu'}|^2}{(\gamma_2 + 2\Gamma_p)^2} \Delta\omega_C$$

where Q_a is the atomic quality factor, $\delta_{\mu\mu'}$ is the hyperfine coherence ($|\delta_{\mu\mu'}| \leq 1/2$) and $\Delta\omega_C$ the cavity detuning. The dependence of k and γ_2 on temperature via the atomic density and of $\Delta\omega_C$ on temperature via the cavity thermal expansion and the electrical permittivity of the cell can limit the medium-long term frequency stability of the clock to few parts of 10^{-12} per degree.

Moreover, for a thick atomic ensemble the dark line in the fluorescence spectrum can appear inverted ("bright line") whereas the EIT signal FWHM is narrower than that predicted by Eq. (8) [73]. Due to this effects and the easier setup required, the transmitted signal is mostly used in the experimental prototypes.

In general, all the above described effects that appear when $\zeta > 1$ (thick sample) increase the sensitivity of the output frequency to the temperature and limit the medium-long term stability.

Concerning the power light-shift, a value of m_ϕ that minimizes the AM-FM conversion still exists, even if relation (10) is no more exact and the signal lineshape becomes slightly asymmetric. Again, for the CPT maser, a new effect appears when the long-wavelength approximation is not satisfied [69]: the **propagation shift** $\Delta\omega_{PS}$, which is an increasing function of the laser intensity I_L but with a sign opposite to that of a pure power light shift, so that it is still possible to find a value of m_ϕ which minimizes the total AM-FM conversion [72] at the level of $(\Delta\nu/\nu)/(\Delta I_L/I_L) < 1 \times 10^{-12}$/%.

We still notice that the three-level system is a rough approximation of the atomic levels involved in CPT and, in addition, the atoms can be excited in a non uniform way. Concerning the first point, we remind that the excited state is homogeneously broadened by buffer gas collisions. This broadening is larger than the hyperfine separation in the excited state so that more levels are simultaneously excited by the optical fields producing CPT.

For example in the case of D_1 line, the two lambda systems shown in Fig. 11 are actually simultaneously excited and the same happens for D_2 line.

The existence of a dark state in those double-Λ systems is basically related to the phases of individual dark states that can interfere constructively or not. On D_1 line, for example, the individual dark states are in phase and sum up producing an overall dark state. Instead, on D_2 transition the two dark states are almost out of phase. Moreover, in D_2 there is a single photon transition that can deteriorate the dark state by depopulation pumping. Definitely, contrasts of CPT resonances observed on D_1 line turn out almost one order of magnitude larger than those observed on D_2 [74, 75]. Dark resonances are also affected by the Zeeman structure in the ground-state. As mentioned in chapter 2, the ground-state degeneracy is removed by applying a magnetic field so that the magnetic insensitive clock transition can be interrogated without interference from the magnetically sensitive transitions. However, these transitions remain close to the clock transition and contribute to absorb the incident laser light, increasing the
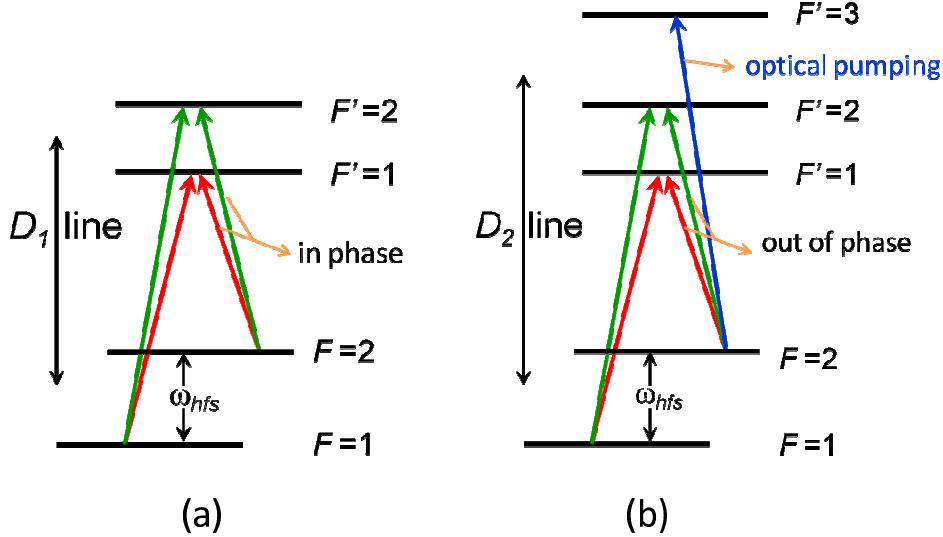
Fig. 11. – D_1 (a) and D_2 (b) lines with levels involved in CPT. In red the original three-level systems and in green the transitions associated to the excited state hyperfine structure. The transition in blue for D_2 acts as optical pumping opposing to the dark state formation.

background level or, om other words, reducing the contrast of the CPT clock resonance. In addition, when circularly polarized light is used a significant fraction of the atoms are pumped towards the so called magnetic end state, as shown in Fig. 12. Due to selection rules these atoms cannot be removed from this trap state (this can be interpreted as an incoherent dark state). Several solutions have been proposed to mitigate this effect [76, 77, 78, 79].

Concerning the non homogeneous interaction, the line shape of dark resonances is sensitive to the laser beam profile that is not uniform but typically has a Gaussian profile; in the high pumping regime this leads to a non Lorentzian profile and consequently also to a linewidth different than that expressed by Eq. (8) [68, 80].

Figure 13 reports the Allan standard deviation asymptotic trends summarizing the most significant results reported in literature with prototypes based on the CPT approach.

Actually, they are not directly comparable since different atoms with different arrangements are used. In all cases, except curve (4), a temperature compensated buffer gas mixture is employed. Curves (3) and (4) refer to a Cs prototype, curve (1) to ^{85}Rb and curves (5) and (6) to ^{87}Rb. As a general behavior, we can say that white frequency noise always dominates the short term stability, as theoretically expected, whereas in the medium term flicker or random walk frequency noises limit the stability in the $10^{-12} - 10^{-13}$ range, with the exception of the CPT maser that, after drift removal, reaches the level of 4×10^{-14} at $\tau = 5000$ s. The CPT approach examined in this subsection reduces the light-shift effect (see tab. I of chapter 5) and allows some improvement of the frequency stability compared to traditional one.
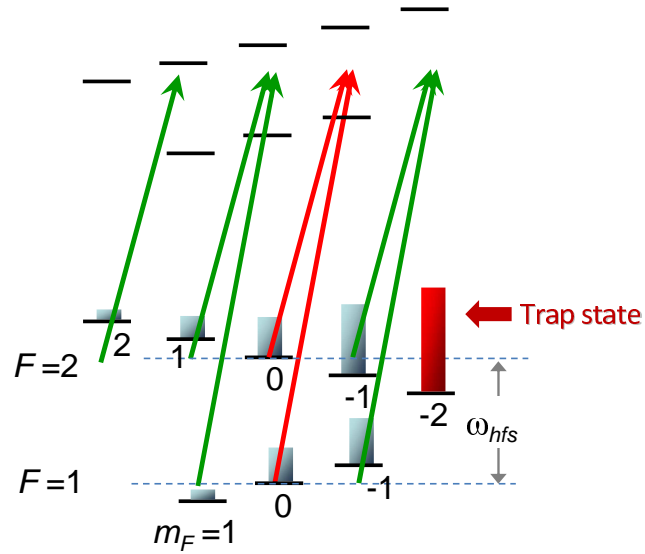
Fig. 12. – Transitions forming dark states in the ground state due to the Zeeman structure in the case of σ^+ polarized light. It is also shown the trap state in which the atoms are pumped by the laser fields.
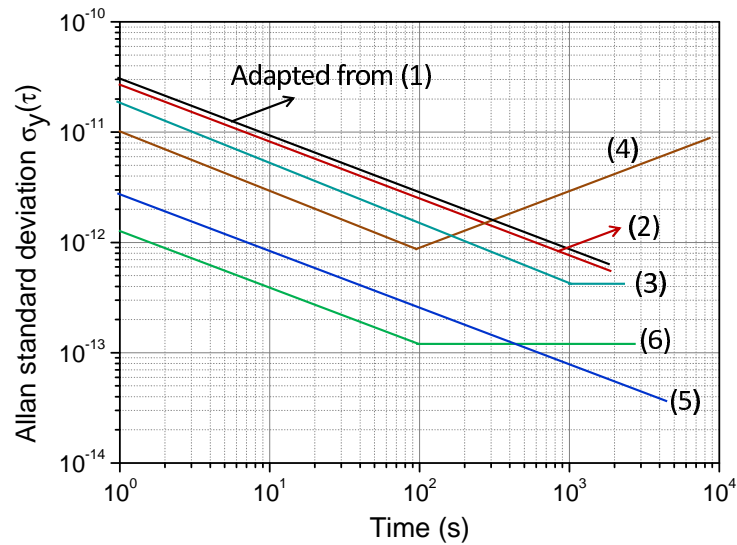

Fig. 13. – Allan standard deviation of CPT based clock prototypes. The curves are adapted from respective references; (1) from [81], (2) from [82], (3) from [83](4) from [84]; (5) from [72]; (6) from [85]; (5) refers to drift removed data coming from the CPT maser.

4'3. *Pulsed EIT standards.* – A vapor cell frequency standard operating in the EIT pulsed mode has been proposed in [86] using a Cs cell; it is based on the Ramsey interrogation technique, performed in the time domain, that allows to observe the atomic resonances with a high Q_a value and with a reference lineshape free of the laser power broadening. Moreover, the interrogation of the clock transition is made in the dark (laser off) so that the light shift is in principle negligible.

In Fig. 14a we report a schematic setup of the pulsed EIT standard. The laser radiations at ω_1 and ω_2, required to implement the Λ scheme, are provided by two independent offset locked lasers. The double Λ scheme (Fig. 14b) is implemented through the lin⊥lin polarized beam; this scheme was first suggested in [76] to significantly increase the contrast of the EIT signal on the background spectrum due to the ground states Zeeman manifold. Recently, it has been demonstrated that the lin⊥lin polarization scheme is identical to the so called push-pull technique [87].
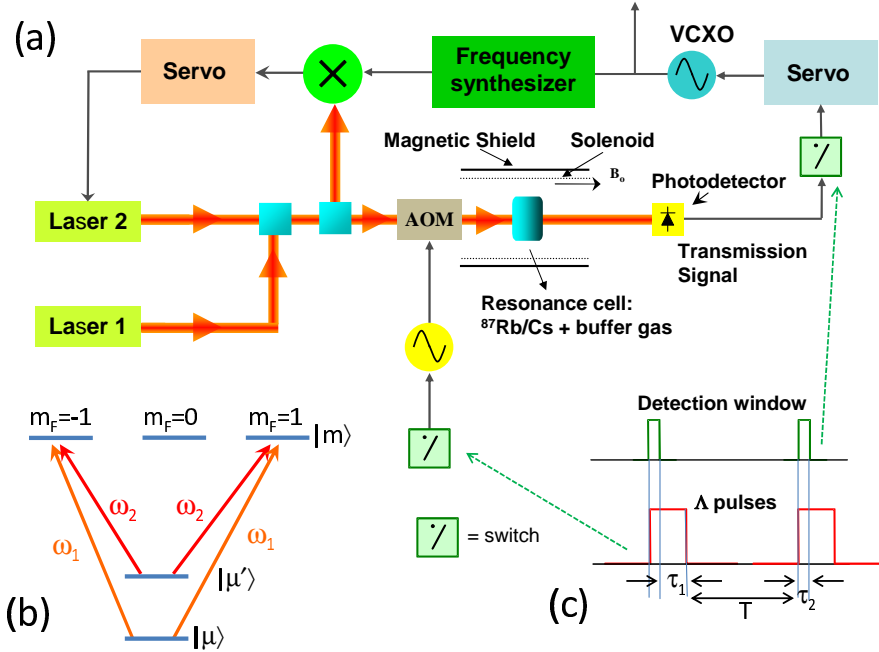

Fig. 14. – (a) Pulsed EIT standard schematic setup; (b) double Λ scheme; (c) timing sequence. Thermal controls of the physics package are not indicated in the figure, as well as the frequency lock of the master laser (laser 1) to the saturated absorption of an external cell containing Rb/Cs vapors

The timing sequence defining the pulsed operation is shown in Fig 14c. Each Λ pulse is used both to prepare and interrogate the atoms. Specifically, the part of duration τ_1 generates the ground states superposition (transversal optical pumping) and pumps the atoms into the dark state. During τ_2 the Λ pulse probes the phase of the dark state after the free evolution phase of duration T. In this scheme, the Ramsey pulses are by definition $\pi/2$ pulses, in fact the CPT scheme is equivalent to an intensity optical pumping process followed by a $\pi/2$ microwave pulse. The detection window must coincide with the second

Ramsey pulse, because only in this case the transmitted optical signal is related to the hyperfine coherence and not to the population inversion that is negligible in CPT.

An efficient pulsed operation mode requires:

$$(13) \qquad \frac{1}{\tau_1} \ll \gamma_2 + 2\Gamma_p \ll \frac{1}{\tau_2}$$

in order to guarantee the dark state preparation and a real detection probe. In the case of a thin atomic medium ($\zeta \ll 1$) with $\omega_{R1} = \omega_{R2} = \omega_R$, $\Delta_0 \ll \Gamma^*/2$ and uniform laser fields profile, an analytical solution for the EIT signal ($\propto \rho_{mm}$) can be found (in the hypothesis of a three-level system the analysis can be simply done with single Λ scheme) [88]:

$$(14) \quad \rho_{mm} = \left(\frac{\omega_R}{\Gamma^*}\right)^2 \left\{ 1 - \frac{2\Gamma_p \, e^{-\gamma_2 T}}{(\gamma_2 + 2\Gamma_p)^2 + \Omega_\mu'^2} \left[(\gamma_2 + 2\Gamma_p)\cos\Omega_\mu T - \Omega_\mu' \sin\Omega_\mu T \right] \right\}$$

where $\Omega_\mu' = \Omega_\mu - \omega_R^2/2\omega_{\mu\mu'}$ is the microwave detuning which accounts for the off-resonant light shift during the Λ pulses. The terms in square brackets describe Ramsey fringes, the Lorentzian expression at their left the Rabi envelope and the exponential term the collisional decay due to buffer gas. The Rabi envelope is centered at $\Omega_\mu' = 0$ and the central Ramsey fringe at $\Omega_\mu = 0$; as a consequence a Rabi pulling is present due to the light-shift during the Λ pulses (τ_1 intervals):

$$(15) \qquad \frac{\Delta\omega/\omega_{\mu\mu'}}{\Delta I_L/I_L} \approx \frac{\Gamma^*}{\omega_{\mu\mu'}^2 T} \frac{\gamma_2 \Gamma_p}{(\gamma_2 + 2\Gamma_p)^2}$$

and for typical operating values it turns out $\frac{\Delta\omega/\omega_{\mu\mu'}}{\Delta I_L/I_L} < 1 \times 10^{-13}/\%$. It could be further reduced with a single phase-modulated laser at the optimum modulation index (see Eq. (10)). In the case of the double Λ scheme the experimental setup is analyzed in [89, 87].

We note from Eq. (14) that the HWHM of the Rabi envelope is $\gamma_2 + 2\Gamma_p$ and that it is not related to τ_1 or τ_2, as expected in the Ramsey technique. Moreover, no resonant light-shift is expected from Eq. (14), which is also valid for $\Delta_0 \neq 0$, if $\omega_{R1} = \omega_{R2}$. In the more practical situation of thick atomic medium $\zeta > 1$ all the above considerations remain still valid. The main effects predicted in this case are the narrowing of the Rabi envelope and of the central Ramsey fringe when ζ increases, and a small broadening of the central Ramsey fringe when the laser intensity increases.

Whatever the value of ζ is, the double Λ scheme excites the $\Delta m_F = 2$ Zeeman transitions, whose pulling effect on the reference transition introduces a magnetic field linear dependence of the output frequency. In practical operating conditions the sensitivity factor is estimated to be $(\Delta\nu/\nu)/(\Delta B_0/B_0) \approx 10^{-10}/\%$ [87, 90].

An experimental prototype of EIT pulsed standard has been developed using a Cs cell with a buffer gas and two phase locked diode lasers tuned to the D_1 line [91, 92]. The frequency stability presently reached is $\sigma_y(\tau) = 3 \times 10^{-13}\tau^{-1/2}$ for $1 \leq \tau \leq 1000$ s [93], after drift removal of $7 \times 10^{-11}/$day. It represents an improvement with respect to the CPT approaches operating in the continuous mode (see also Tab1), and to date

is the best CPT clock ever realized. The clock midterm frequency stability is mainly limited by buffer gas related temperature shift, unbalance between laser field intensities and frequency pulling by $\Delta m_F = 2$ Zeeman transitions; further theoretical and experimental works is in progress to improve this stability currently reached and exploit the full capabilities of this standard.

5. – Pulsed Optically Pumped standards

The development of semiconductor lasers and pulsed electronics for atomic fountains, together with new theoretical results, allowed to reconsider the idea of pulsed optical pumping (POP) [94] originally conceived by Alley [95] and first applied to the field of frequency standards by Arditi and Carver [96].

The POP clock concept relies on three operation phases. First, a strong laser pulse generates an imbalance between the two ground-state levels through optical pumping. Then, the interrogation of the reference transition takes place fully in the dark with a temporal Ramsey technique. Finally, the atoms that have made the clock transition are detected. Analogously to the CPT standards, the detection of the hyperfine reference transition can occur in the microwave domain, through the free-induction decay signal (POP maser), or in the optical domain, through the transmitted optical signal.

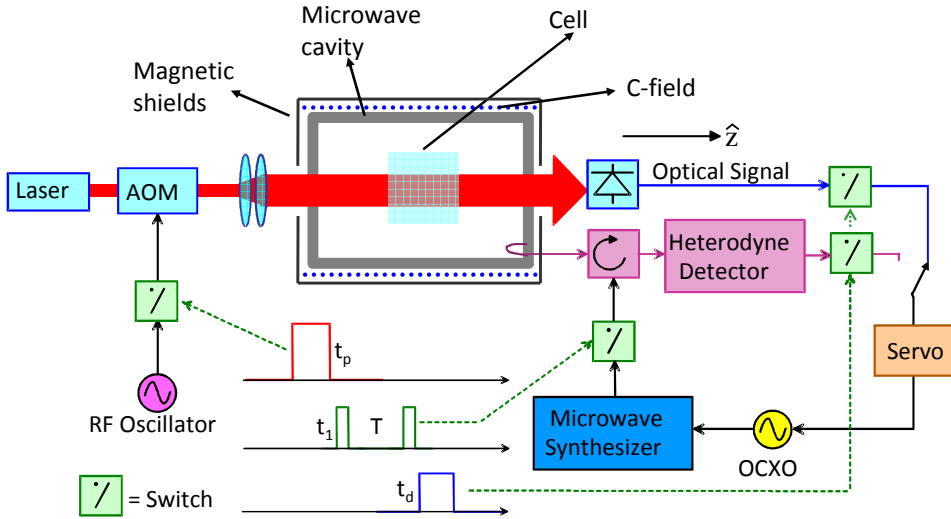The schematic setup of the POP frequency standard is shown in Fig. 15.

Fig. 15. – Schematic setup of the POP frequency standard; AOM acousto-optic modulator; t_p, t_1, T and t_d are respectively the pumping, Rabi pulses, Ramsey and detection times.

The simplified scheme of the levels involved is the same of Fig. 2 but now laser and microwave fields are alternatively applied. The multilevel scheme including the Zeeman manifolds of the hyperfine ground states and of the excited optical state has been considered in [26, 97] to quantitatively describe the optical pumping process and in particular the initial conditions for the microwave interrogation. The clock dynamics can be formally reduced to that of a two-level system $|\mu\rangle$, $|\mu'\rangle$ for the mi crowave interrogation

and $|\mu'\rangle$, $|m\rangle$ for the detection and the optical pumping; all these phases are well separated in time as indicated by the timing patterns of Fig. 15.

To give more physical insight into the POP approach, we consider the hyperfine coherence at the end of a laser pumping pulse $\delta_{\mu\mu'}(t_p)$ which is related to its initial value $\delta_{\mu\mu'}(0)$ at the beginning of the same pulse by the following relation [97]:

$$(16) \qquad \delta_{\mu\mu'}(t_p) = \delta_{\mu\mu'}(0)e^{-(\gamma_2+\Gamma_p)t_p}e^{-i(\Omega_\mu-\Gamma_p\delta_0-\omega_R^2/4\omega_{\mu\mu'})t_p}$$

where $\delta_0 = 2\Delta_0/\Gamma^*$ is the reduced laser detuning. Equation (16) holds for a thin atomic medium ($\zeta \ll 1$).

It is evident from Eq. (16) that in order to avoid any phase memory among consecutive cycles, and then the light-shift effect contained in the rotating term, it is necessary to satisfy the condition $\Gamma_p t_p \gg 1$. In the case of an optical thick medium this condition becomes [94]:

$$(17) \qquad (\Gamma_p - \zeta\gamma_1)\,t_p \gg 1$$

In other words, when Eq. (17) is satisfied, the atoms do not experience any laser light while doing the clock transition, therefore light-shift becomes negligible. It is important to point out that while in CPT and in pulsed EIT (see Eq. 15) the light-shift compensation occurs in one single operation point, in the POP technique the condition that must be satisfied is an inequality on the laser pumping rate and this is much easier to be fulfilled from an experimental point of view. In practice, as we will see later, there is still a residual light shift component due to the coherence not completely extinguished by the laser at the beginning of a new cycle.

5$\cdot$1. *The POP maser*. – In the POP maser, the microwave power dissipated in the cavity can be observed through a spectrum analyzer when the atomic sample is placed in a high-Q cavity. In Fig. 16, it is possible to distinguish the two microwave pulses defining the Ramsey scheme, the free induction decay signal between them and the clock signal that is just after the second microwave pulse at the beginning of the detection interval [97].

We notice the fast decay of the signal after the detection; this is due to the coherence destruction caused by the laser pumping pulse: the laser pulse not only inverts the population in the ground state but at the same time resets the the atomic phase, so that the atoms start a new cycle without any memory of the laser interaction.

For a fixed microwave frequency, the clock signal is the area highlighted in Fig. 16. By varying the microwave detuning, it is possible to observe the full pattern of Ramsey fringes. In the specific case of Fig. 17, Ramsey fringes have been obtained for the following timing: $t_p = 1$ ms, $t_1 = 400$ μs, $T = 4.6$ ms, $t_d = 2$ ms and $\Gamma_p = 120000$ s^{-1}. In addition, the microwave power is set in such a way that the microwave pulse area $\theta = b_e t_1$ is equal to $\pi/2$.

The central fringe of the Ramsey pattern is shown in Fig. 18 and can be written as:

$$(18) \qquad P_a = \frac{1}{2}\hbar\omega_{\mu\mu'}N_a k|\Delta_i|^2\ e^{-2\gamma T}\left[\tanh^2 A(T) + \operatorname{sech}^2 A(T)\sin^2\Omega_\mu T\right]$$
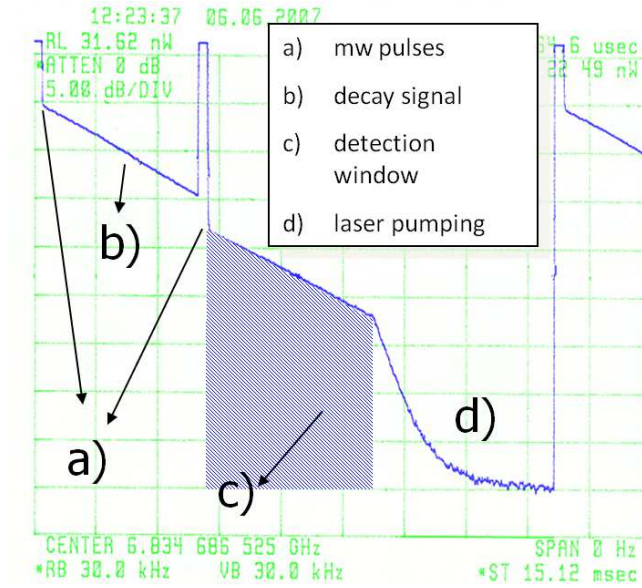
Fig. 16. – Free induction decay observed at the cavity output; $t_p = 4$ ms, $t_1 = 400$ μs, $T = 4.6$ ms, $t_d = 4$ ms.
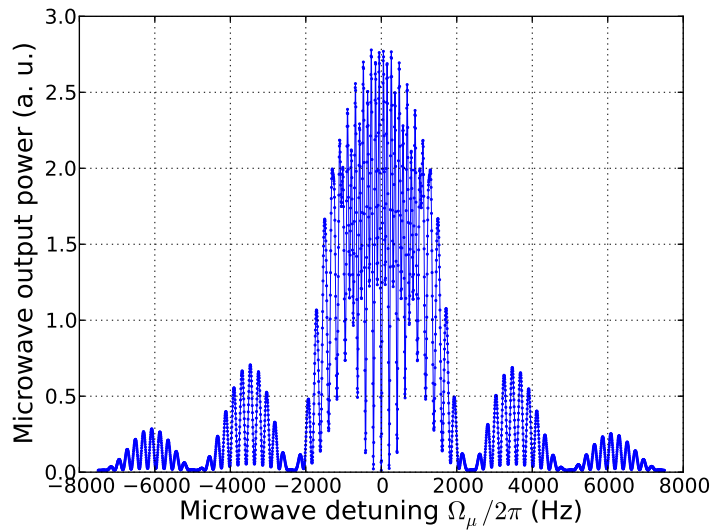

Fig. 17. – Full pattern of interference Ramsey fringes.

when $\gamma_1 \approx \gamma_2 = \gamma$ and where Δ_i is the ground state population inversion at the end of the laser pumping pulse and $A(T) = (\frac{k}{\gamma})|\Delta_i| \left(1 - e^{-\gamma T}\right)$. The square brackets describe

the central Ramsey fringe for $\pi/2$ microwave pulses, whose FWHM turns out $\Delta\nu_{1/2} = 1/4T$ and whose amplitude is reduced by the radiation damping factor $\mathrm{sech}^2 A(T)$. The linewidth of the central fringe is then 54 Hz, corresponding to an atomic quality factor $Q_a \approx 1.2 \times 10^8$.
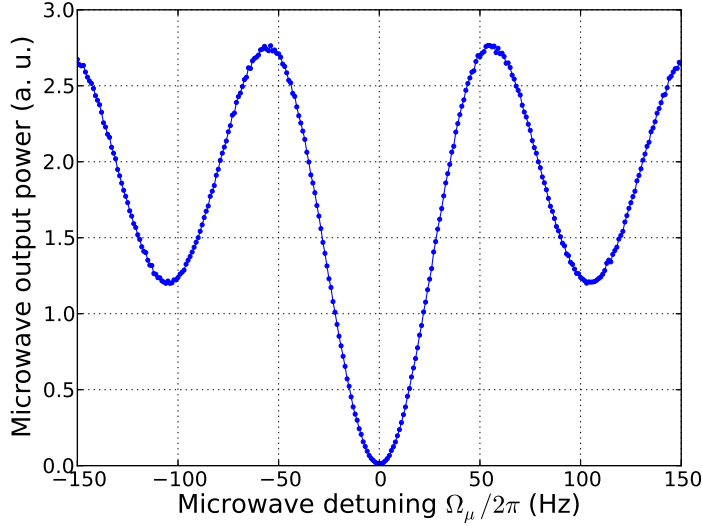

Fig. 18. – Central fringe of the Ramsey pattern shown in the previous figure.

The frequency stability of the POP maser is reported in Fig. 20 where is compared with the stability obtained with the optical detection.

5˙2. *The POP clock with optical detection*. – The optical detection of the clock transition exhibits some advantages compared to the maser approach. Due to the higher energy carried by optical photons, a better signal-to-noise ratio is expected. This results in an improving of the short-term frequency stability. In addition, some requirements concerning the cavity are relaxed. Since the cavity plays a role only during the interrogation and not in the detection phase, it is not necessary to have a very high cavity quality factor which is fundamental in the maser approach ($Q_L \approx 5000 \div 10000$). A $Q_L \approx 1000$ or less can be sufficient to operate the clock in the optical detection mode.

The reference signal is provided by the transmission laser pulse of duration t_d detected at the end of the cell $\propto \Gamma'_p(L)$ [98]:

$$(19) \qquad \Gamma'_p(L) = \Gamma'_p(0)e^{-\zeta}\left[I_0(\chi) + 2\sum_{m=1}^{\infty} I_m(-\chi)\cos(m\Omega_\mu T)\right]$$

where $\Gamma'_p(0)$ is the laser pumping rate in the detection phase at the cell input; this "probe pulse" is expected not to change the population inversion, so that the following condition must be fulfilled:

(20) $$\left[\gamma_1 + \Gamma_p'(0)\right] t_d \ll 1$$

In Eq. (19) $\chi = \zeta(n_{eff}/n)_p\ e^{-\gamma_2 T}$, $(n_{eff}/n)_p$ is the fraction of atoms effectively pumped in the $m_F = 0$ clock states and $I_m(x)$ the modified Bessel functions of the first type. For an optically thin medium the shape of the central Ramsey fringe reduces to $\cos\Omega_\mu T$ with a FWHM $\Delta\nu_{1/2} = 1/2T$ and the behavior of the contrast C is given by [18]:

(21) $$C \propto \frac{\hbar\omega_L Z_0(d_e/\hbar)^2}{\Gamma^*}\frac{N_a}{S}\Delta_i e^{-\gamma_2 T}$$

where Z_0 is the vacuum characteristic impedance, S the section of the interaction zone and d_e the electric dipole moment of the optical transition. The contrast is then proportional to d_e^2 (in this regard, D_2 is then better than D_1 in the detection phase due to its higher d_e) and is nearly independent of $\Gamma_p(0)$ and t_d.

A more complete theoretical description of the POP frequency standard based on a multilevel approach is reported in [26].

Similarly to the maser approach, it is possible to observe Ramsey fringes scanning the microwave frequency around the resonance. Figure 19 shows Ramsey fringes for a cell temperature of $T = 68\ ^oC$, a laser pumping power of 15 mW (corresponding to a pumping rate of $8.5 \times 10^5\ s^{-1}$) and a laser detection power of 1 mW ($5.6 \times 10^4\ s^{-1}$).
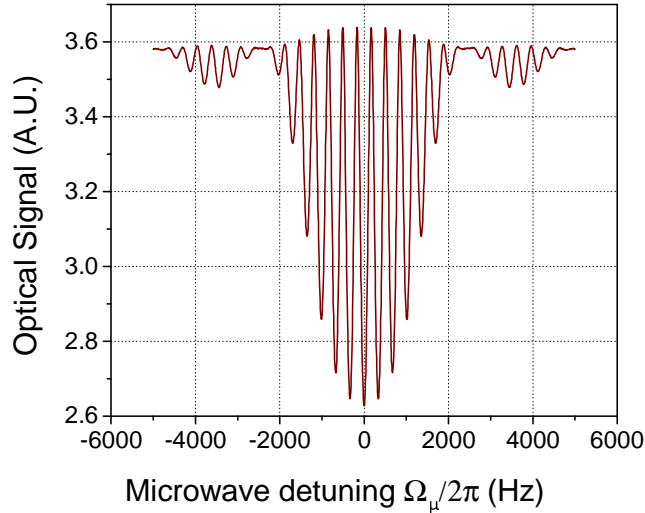
Fig. 19. – Ramsey pattern observed in the optical detection mode. The timing of the different operation phases is: $t_p = 0.44$ ms, $t_1 = 0.4$ ms, $T = 3.3$ ms and $t_d = 0.15$ ms.

The central fringe of Fig. 19 exhibits a contrast of 28% and a linewidth of about 150 Hz, corresponding to a quality factor of 4.5×10^7. In Ref. [18] a complete characterization of the contrast has been reported. Indeed, the contrast plays a key role not only to

determine the signal level but also to reduce some noise sources, as it will be explained in more detail in chapter 6.

We mention that a POP clock prototype operating in the optical detection mode and using a compact magnetron-type microwave cavity is under development at the University of Neuchatel [99].

5˙3. *Frequency shifts and stability performances*. – As mentioned at the beginning of this chapter, the pulsed optical pumping reduces light-shift to a residual level. Specifically, this residual light-shift is due to the limited laser intensity in the pumping phase and turns out [97]:

$$(22) \qquad \frac{\Delta\omega_{LS}}{\omega_{\mu\mu'}} = \frac{2(\theta - \pi/2)}{\pi Q_a} \frac{(\delta_0 - \Gamma^*/2\omega_{\mu\mu'})\Gamma_p t_p}{1 + \cosh(\gamma_2 T_C + \Gamma_p t_p)}$$

where θ is the microwave pulse area, b_e its microwave Rabi frequency and T_C the cycle time. Equation (22) predicts a full elimination of the light shift effect when $\theta = \pi/2$. In the more realistic case $|\theta - \pi/2| \leq 0.1$ with $\Gamma_p t_p \approx 5$, the AM-FM and FM-FM conversion factors in practical operating conditions are expected lower than $1 \times 10^{-14}/\%$ and $1 \times 10^{-14}/\mathrm{MHz}$ respectively.

The inhomogeneities in the atomic sample, mainly due to the non-uniformity of the RF field of the cavity mode, to the laser absorption and to the laser mode, introduce a residual coupling between optical and microwave signals so that the clock frequency still exhibits a dependence on the laser power. This effect, first discussed in [100], is known as **positioning shift** or **pseudo light shift** because it mimics the off resonant light shift behavior; even if its contribution to the AM-FM conversion factor can be reduced below $1 \times 10^{-13}/\%$ [26], an intensitiy stabilized laser is required in order not to deteriorate the clock medium-long term stability. The above shift vanishes when $k = 0$ or $\Delta\omega_C = 0$ (we remind that k is the cavity feedback parameter defined at p. 13 and $\Delta\omega_C$ the cavity detuning versus the atomic frequency introduced at p. 16. This behaviour, similar to the cavity pulling effect, is a consequence of the coupling between laser and microwave fields introduced by the position shift.

The **cavity pulling shift** $\Delta\omega_{CP}$ is the direct consequence of the cavity feedback on the atomic ensemble; in the limit of small cavity detuning we have:

$$(23) \qquad \Delta\omega_{CP} = \frac{4}{\pi} \frac{Q_L}{Q_a} c(\theta)\Delta\omega_C$$

where the function $c(\theta)$ is reported in [94, 97]; it is minimized for $\theta \approx \pi/2$.

The more relevant contribution of the cavity pulling effect to the clock frequency instability is due to the sensitivity to the microwave power $P_{\mu w}$ (**microwave power shift**), that can reach the value $(\Delta\nu/\nu)/(\Delta P_{\mu w}/P_{\mu w}) \approx 1 \times 10^{-13}/\%$ and then require an active system to stabilize the microwave power (we remind that $P_{\mu w} \propto \theta^2$).

In Fig. 20 we report the Allan standard deviations obtained with prototypes based on the POP approach. Curve (a) refers to a POP maser [26] after a drift removal of $8 \times 10^{-14}/\mathrm{day}$ and curve b) to a POP prototype operating in the optical detection mode [18] after a drift removal of $8 \times 10^{-15}/\mathrm{day}$. In both cases, the clock signal is affected by white frequency noise and the Allan deviation scales as $\tau^{-1/2}$. We notice the improvement of one order of magnitude of the optical detection compared to the microwave one.
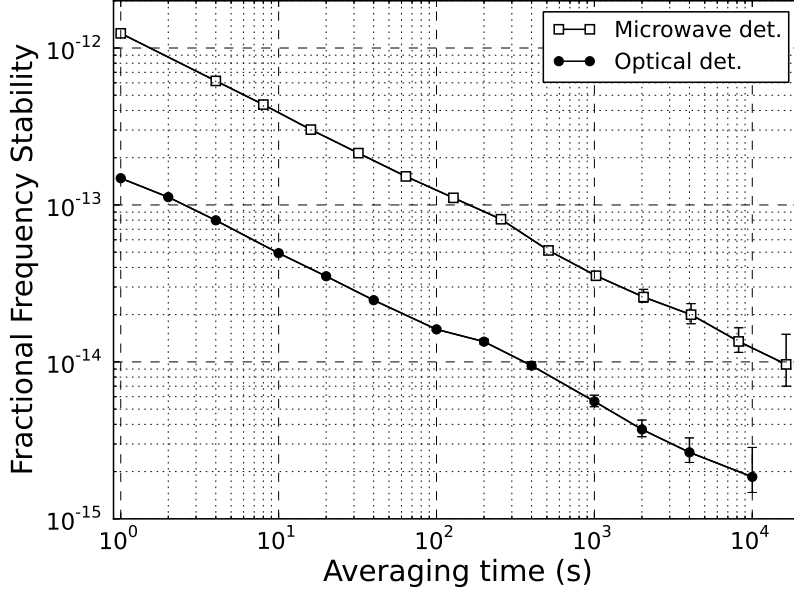
Fig. 20. – Allan standard deviation for the POP maser (white square) and for POP optical detection mode (black circle).

The stability of the POP clock with optical detection shown in Fig. 20 refers to a subset of 50000 points extracted from a larger sample; the selected subset corresponds to the period where environmental parameters, the temperature in particular, were more stable. Figure 21 shows the POP clock stability using the complete sample of data corresponding to a measurement run of 12 days. Notably, we point out the long-term stability remains below the 10^{-14} level for integration times up to 10^5 s.

The light and microwave shifts experimentally observed are reported in Table 1 for comparison with the other approaches and are no more the limiting factors of the achieved stability. Specifically, for the POP operating in the optical detection mode, the short-term stability turns out to be limited by the laser noise transferred to the amplitude of the clock signal. The other main instability source comes from the phase noise of the interrogating microwave. In the medium-long term period the performances are mainly limited by the instability and non-homogeneity of the cell temperature.

As a conclusion of this chapter, the following points are outlined: i) the pulsed operation mode is more effective than the continuous case to reduce the light and microwave shifts; ii) the optical detection mode allows to reach a better short term frequency stability; moreover, it requires a lower cavity quality factor or no cavity at all in the pulsed EIT case, but also a better control of the laser amplitude and frequency noises to avoid AM-AM and FM-AM contributions in the detection phase [26, 18].

In the following sections we will analyze the laser noise contribution, the Dick effect and the temperature effects that limit the stability independently of the chosen technique and possible solutions proposed to reduced them in order to further approach the
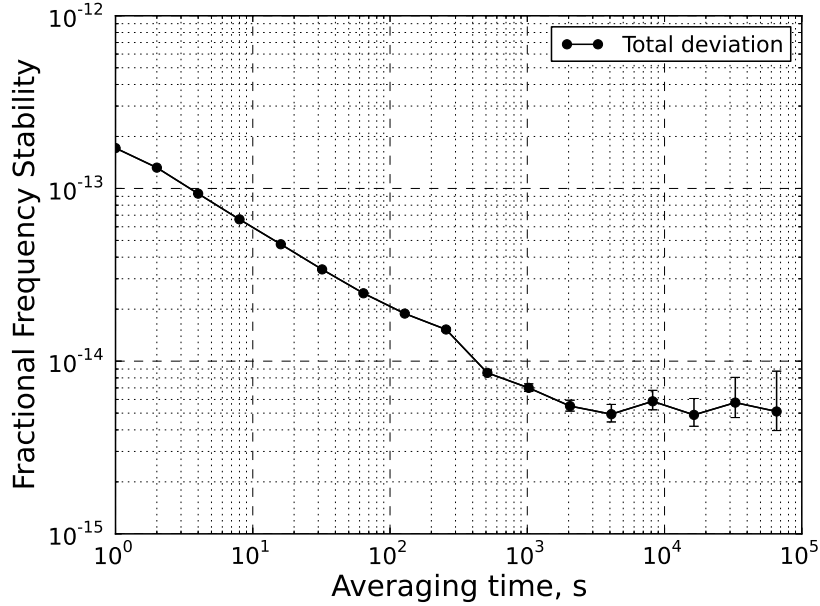
Fig. 21. – Medium-long term measurement of POP clock frequency stability.

theoretical limit not yet achieved until today.

6. – Laser and microwave noise

The laser frequency and amplitude noise in the detection phase limits the frequency stability of the clock operating in the optical detection mode. The amplitude fluctuations

Clock technique	Frequency light-shift $(\Delta\nu_{LS}/\nu)$ /MHz	Intensity light-shift $(\Delta\nu_{LS}/\nu)$ /%	Microwave power shift $(\Delta\nu_{\mu w}/\nu)$ /%
Double-resonance (CW) [25]	$(1 \div 10) \times 10^{-11}$	$(1 \div 10) \times 10^{-11}$	1×10^{-13}
Continuous CPT [72, 83, 81]	$(0.5 \div 2) \times 10^{-12}$	$< 1 \times 10^{-12}$	not applicable
Pulsed CPT [87, 91]	7×10^{-13}	$< 1 \times 10^{-13}$	not applicable
POP [18, 97, 98]	$< 2 \times 10^{-14}$	$< 1 \times 10^{-13}$	1×10^{-13}

TABLE I. – *Typical observed sensitivities of the different approaches considered in the text; under each clock approach the respective references are indicated.*

of the probe field reaching the photodetector add an additive noise whose contribution to the clock Allan deviation can be expressed as [26]:

$$(24) \qquad \sigma_y(\tau) = \frac{1}{CQ_a} \left\{ \sum_{k=1}^{\infty} \text{sinc}^2 \left(k\pi \frac{T}{T_C} \right) S_{AM}(kf_c) \right\}^{1/2} \tau^{-1/2}$$

where T_C is the cycle time, $f_c = 1/T_C$ and $S_{AM}(f)$ the power spectral density of the fractional intensity fluctuations of the laser field reaching the photodetector. It contains both the laser AM noise transferred to the output of the cell (AM-AM) and laser FM noise converted into amplitude fluctuations (FM-AM) via interaction with the atomic sample.

For typical experimental conditions ($C \approx 30\%$, $Q_a \approx 5 \times 10^7$, $T/T_C \approx 0.7$, $S_{AM}(f) \approx 2 \times 10^{-11}$ Hz^{-1} for 100 Hz $< f <$ 1 kHz) Eq. (24) predicts $\sigma_y(\tau) \approx 1 \times 10^{-13} \tau^{-1/2}$. In order to improve this limit it should be required to increase the contrast and to reduce significantly the laser noise contribution. From this point of view, the detection of the clock transition through the magneto-optical rotation effect, proposed by the Y. Z. Wang's group [101], appears very attractive for the POP approach.

The schematic setup of Fig. 15 is simply modified by inserting the cell between two cross polarizers: the detected scattering signal resulting from magneto-optical rotation carries the Ramsey pattern information with a contrast of up to 90% and an improved signal-to-noise ratio due to rejection of the laser background. The experimental results reported in [101] foresee a possible improvement of the stability limit due to the laser noise by an order of magnitude with respect to the absorption detection technique.

In passive frequency standards the phase noise of the microwave interrogating signal limits the achievable frequency stability, as recognized for the first time by G. Kramer [34]. also known as Dick effect. In frequency standards working in the pulsed operation mode, the phase noise of the interrogating signal manifests as Dick effect and is given by [102, 103, 104]:

$$(25) \qquad \sigma_y(\tau) = \left\{ \sum_{k=1}^{\infty} \text{sinc}^2 \left(k\pi \frac{T}{T_C} \right) S_y^{LO}(kf_c) \right\}^{1/2} \tau^{-1/2}$$

where $S_y^{LO}(f)$ is the power spectral density of the microwave fractional frequency fluctuations. The low phase noise microwave synthesizer designed for the POP clock [18] leads to a Dick effect limited stability $\sigma_y(\tau) \approx 7 \times 10^{-14} \tau^{-1/2}$, state of the art synthesizers and local quartz oscillators can reasonably reduce this limit by a factor of 2, leaving anyway the Dick effect as the main limitation for the short term frequency stability of the clock [105].

A significant improvement could be achieved in the limit $T/T_C \to 1$, that is in the zero dead time operational conditions, as it turns out from Eq. (25), but this would strongly deteriorate the shot noise theoretical limit. To overcome these problem Biedermann et al. suggested a zero dead time operation of interleaved atomic clocks [106]. The principle is reported in Fig. 22.

Two identical POP physics packages (for example) are interrogated by the same microwave synthesizer (Fig. 22a) with Ramsey pulses synchronized in such a way that the combined operation of the two clocks is dead time free (Fig. 22b). This technique allows
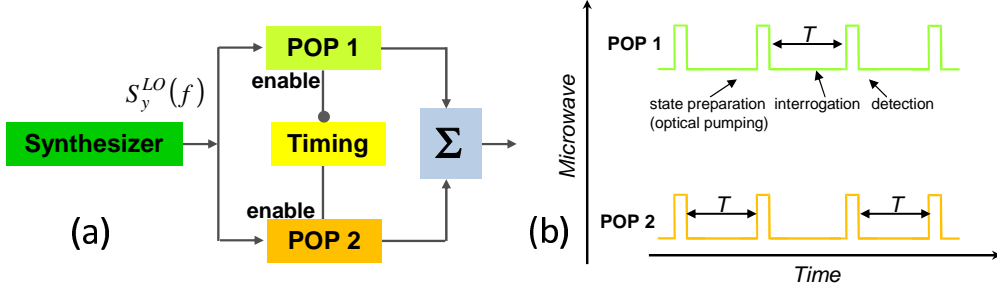
Fig. 22. – Interleaved atomic clocks: a) basic setup; b) $\pi/2$ microwave pulses timing (adapted from [106]).

an improvement of the short term stability due to the microwave phase noise, which now averages as $1/\tau$ down to reach the shot-noise limit, as it has been experimentally demonstrated in the case of two atomic fountain clocks. We remind that, as suggested in p. 6, two physics packages can be also used to implement a subtraction of the laser noise transferred to the atoms. The two techniques could then be combined to simultaneously reduce Dick effect and laser noise conversion. The double physics package approach then appears very promising to improve the short-term frequency stability and deserves further investigation.

7. – Medium-long term

In any atomic frequency standards the clock resonance is influenced by several effects that produce a shift of the output clock frequency with respect to the unperturbed transition. In particular, for a vapor cell clock the output frequency ν_0 can be written as:

$$(26) \qquad \nu_0 = \nu_{hfs} + \Delta\nu_{B0} + \Delta\nu_{bg} + \Delta\nu_{se} + \Delta\nu_{cp} + \Delta\nu_{ls}$$

where ν_{hfs} is the unperturbed hyperfine frequency and the other terms are the frequency shifts due respectively to the (second order) Zeeman effect, the ^{87}Rb-buffer gas collisions, the spin-exchange (^{87}Rb-^{87}Rb collisions [107]), the cavity pulling and the light-shift.

Some of these shifts are inherent to the cell itself, they are then common to all vapor cell clocks. Others may not be present in some arrangements: $\Delta\omega_{CP}$ is of course absent in CPT (with optical detection) since the cavity is not needed.

Equation (26) expresses the fact that the fluctuations of several physical quantities can be transferred to the clock transition through different physical effects, as pictorially illustrated in Fig. 23.

For instance, the clock transition frequency is affected by temperature fluctuations via buffer gas (see later) and spin-exchange collisions and through the cavity pulling.

Since vapor cell frequency standards are intrinsically not accurate, the exact amount of these shifts is not an issue. Rather, we are interested to evaluate how these shifts
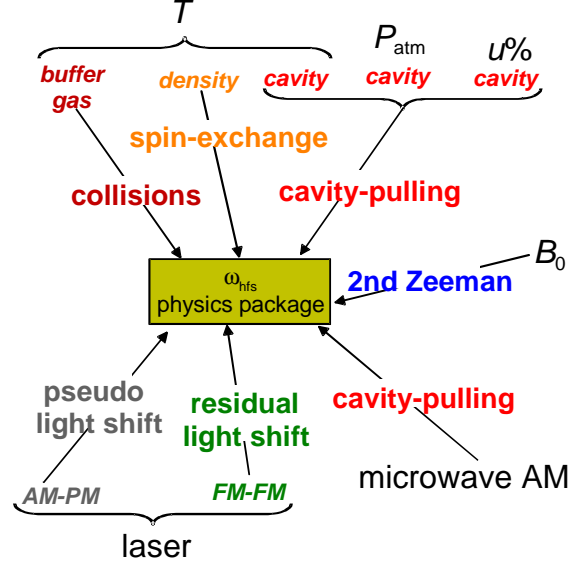
Fig. 23. – Noise sources affecting the clock transition frequency through the indicated physical effects; P_{atm} is the barometric pressure and $u\%$ is the relative humidity. The other quantities are defined in the text.

change versus the variations of the physical quantities they depend on. In other words, we must evaluate for each shift the corresponding sensitivity coefficient so that it is known at which level a given physical quantity must be kept constant in order to get a certain level of frequency stability.

We do not discuss here each shift reported in Eq. (26). A more detailed analysis of the medium-long term frequency stability has been examined in detail in [54] for the continuous DR clock, in [108] for the POP approach and in [90] for the pulsed CPT clock.

In this review, we remind the buffer gas shift that is common to all the approaches here described and, in addition, it is related to the enhanced temperature sensitivity (ETS) effect described only recently.

The atom-buffer gas collisions produce a shift $\Delta\nu_{bg}$ of the hyperfine transition [4] that can be modelized by:

$$(27) \qquad\qquad \Delta\nu_{bg} = P_s \left[\beta + \delta(T - T_0) + \gamma(T - T_0)^2\right]$$

where P_s is the total buffer gas pressure, β the pressure coefficient, δ and γ the linear and quadratic temperature coefficients, T the working temperature (not to be confused with the Ramsey time) and T_0 is a reference temperature around which the coefficients are measured.

A mixture of buffer gases can be chosen with the purpose of making negligible the linear temperature coefficient at a certain inversion temperature T_i, in this case, referring the parabola coefficients to T_i, we can write [109]:

(28)
$$\Delta\nu_{bg} = P_s \left[\beta_i' + \gamma_i'(T - T_i)^2 \right]$$

where β_i' and γ_i' are usually obtained by a parabolic fit of the experimental data. In the absence of any temperature inhomogeneity, the clock temperature sensitivity is:

(29)
$$\frac{\partial(\nu/\nu_{\mu\mu'})}{\partial T} = \frac{2P_s\gamma_i'}{\nu_{\mu\mu'}}(T - T_i)$$

Unfortunately, Eq. (29), always adopted in the scientific literature, provides a too optimistic estimation of the temperature sensitivity. In fact, temperature inhomogeneities, mostly between the cell (maintained at temperature T_a) and the stems (T_b), play an important role and the proper temperature sensitivity is given by [109]:

(30)
$$\frac{\partial(\nu/\nu_{\mu\mu'})}{\partial\Delta T} = -\frac{P_s\beta_i'v_b}{\nu_{\mu\mu'}T_b}$$

where $\Delta T = T_a - T_b$ and v_b is the relative volume of the part of the cell outside the cavity.

This ETS effect is not due to changes in the interaction between Rb and buffer gas atoms, but it is a purely geometrical effect related to a buffer gas density variation between the cell body and the stem volumes. The effect of the stem temperature on the clock frequency stability over a period of one day or longer is investigated in [110]

To reduce the temperature sensitivity below 10^{-10}/K predicted by Eq. (30) for typical cell designs, it is required to minimize as much as possible v_b and, unexpectedly, the pressure coefficient β_i' (with three different buffer gases, for example); only at that point Eq. (29) prediction becomes meaningful.

The cavity pulling effect introduces a sensitivity of the clock frequency on the barometric pressure fluctuations, on the cavity temperature, on the microwave power and on the laser intensity. The first one can be avoided operating the physics package in vacuum, whereas the second can be reduced, for example, using a Mo cavity. The sensitivities on the microwave power and on the laser intensity (pseudo-light shift) take benefit, obviously, from a low cavity Q-factor; in particular, the last shift can be lowered reducing the inhomogeneities in the atomic sample. A more complete analysis is reported in [108] and [111].

In general the cavity pulling related effects can be controlled via a proper design of the cell-cavity system to allow a medium long term frequency stability in the low 10^{-15} range, leaving the buffer gas related temperature shifts as the main responsible of the instabilities in the medium long term.

8. – Cold atoms vapor cell clock

So far we considered vapor cell clocks based on hot samples of atoms. However, very recently, a cell clock based on cold atoms has been implemented. The clock works thanks to isotropic cooling of the atomic vapor inside a spherical cavity, so that it is possible to observe the hyperfine clock transition without any Doppler broadening. Moreover, no

buffer gas is used to localize the atoms and a number of relaxation effects, such as buffer gas and cell wall collisions, is avoided.

The feasibility of atom laser cooling with an isotropic light, first considered in [112, 113], was experimentally demonstrated with a cylindrical diffusive material used to slow a Na atomic beam [114]. The isotropic cooling of a Cs vapor sample inside a cylindrical cell at the temperature of 3.5 μK was reported in [115]. The above basic works led to the research program of N. Dimarcq and coworkers named HORACE whose very interesting properties are reported in [116]. In HORACE, an atomic Cs vapor is isotropically cooled inside a spherical cavity used also as integrating sphere, as first suggested in [117].

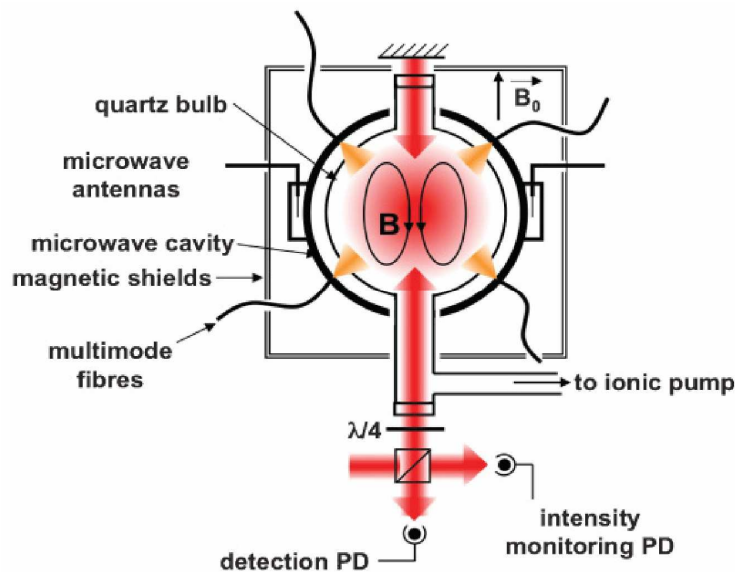The scheme of the physics package is shown in Fig. 24.

Fig. 24. – Physics package of HORACE. Reprinted figure with permission from: F. -X. Esnault, D. Holleville, N. Rossetto, S. Guerandel and N.Dimarcq N., Phys. Rev. A 82,033436, 2010. Copyright 2012 by the American Physical Society.

The core of the clock is a copper spherical microwave cavity resonating on the TE_{110} mode [111] tuned to the hyperfine clock transition and fed by two symmetric antennas. The atomic vapor is contained in a blown quartz bulb to prevent the interaction of the cavity walls with Cs atoms. The cavity acts as an integrating sphere for the 852 nm laser radiation injected via six multimode fibers. A simple Doppler cooling sequence allows to cool the atoms to a temperature of about 35 μK. After the cooling phase, the operation of HORACE is very similar to that of the POP clock. Once the cooling lasers are switched off, the atoms are optically pumped into the clock level $|F = 3, m_F = 0\rangle$. The atoms fall by gravity and during this free fall experience two microwave pulses according to the Ramsey scheme. The Ramsey time is then limited by gravity to 25 ms, resulting in clock transition linewidth of 18 Hz. A vertical retro-reflected laser beam probes the atoms in order to detect the clock transition. Ramsey fringes of the HORACE clock are reported in Fig. 25.
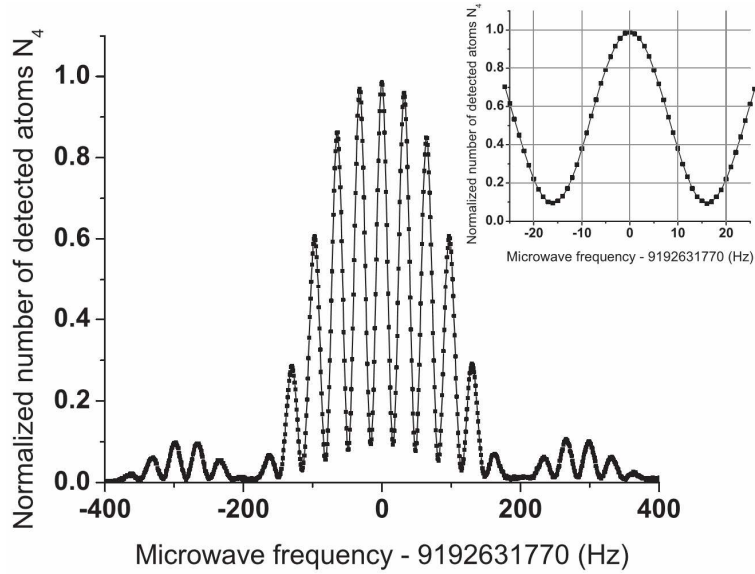
Fig. 25. – Ramsey fringes observed in HORACE; the inset shows the central fringe of the Ramsey pattern. N_4 is the number of detected atoms in level $|F = 4, m_F = 0\rangle$. Reprinted figure with permission from: F. -X. Esnault, D. Holleville, N. Rossetto, S. Guerandel and N.Dimarcq N., Phys. Rev. A 82,033436, 2010. Copyright 2012 by the American Physical Society.

We point out that the isotropically cooled vapor cell standard exhibits in principle some advantages compared to the approaches so far considered. In particular:

a) the absence of a buffer gas eliminates the temperature related shifts, which are recognized as the source of the residual medium-long term frequency instability, as discussed in the previous chapter. In addition, it is possible to make an evaluation of the accuracy budget; specifically, the expected accuracy level is in the low 10^{-14} region; b) As in atomic fountains, the atomic cloud is renewed at every cycle, no phase memory exists between consecutive cycles and then in principle there is no light-shift. The only possible source of light-shift is the laser leakage during the Ramsey interaction. However, this effect in similar structures has been evaluated well below the 10^{-15} level [118]; c) the atomic sample is very thin so that the cavity pulling, the microwave power shift and the position-shift effects turn out strongly reduced, below 10^{-16} [119]. Moreover, being the medium very diluted, the FM-AM laser noise conversion in the detection phase is nearly absent, relaxing the laser frequency requirements.

In terms of frequency stability, Fig. 26 shows that the Allan deviation is as low as $2.2 \times 10^{-13}\tau^{-1/2}$ and scales as white frequency noise up to 2000 s, reaching the 4×10^{-15} level for an integration time of 5000 s.

An analysis of the effects limiting this result shows that the short-term stability is limited by the atomic shot noise.

Since HORACE, as the other clocks based on cold atoms, can provide the accuracy information, it is of fundamental importance to reduce as much as possible all the effects that can shift the clock resonance frequency. In this regard, one of the main limiting phenomena is the density shift due to collisions among Cs atoms. A clock based on the
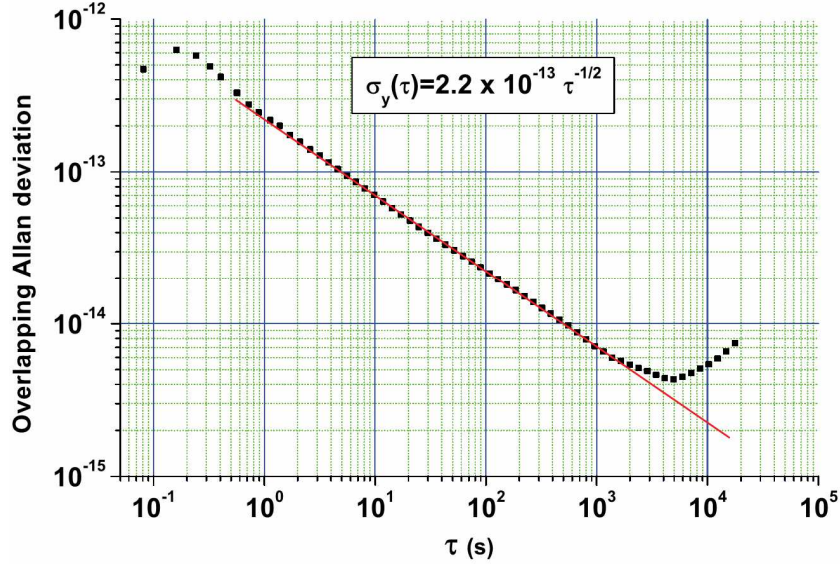
Fig. 26. – Frequency stability of the HORACE clock; a cryogenic sapphire oscillator locked to a H-maser is used as frequency reference. Reprinted figure with permission from: F. -X. Esnault, D. Holleville, N. Rossetto, S. Guerandel and N.Dimarcq N., Phys. Rev. A 82,033436, 2010. Copyright 2012 by the American Physical Society.

HORACE principle but with ^{87}Rb has then been implemented (RUBICLOCK). It is in fact well known that ^{87}Rb has a collisional cross section of about two order of magnitude smaller than that of Cs. Preliminary results of RUBICLOCK operating in microgravity conditions have been presented in [21].

9. – Conclusion

We have reported in this paper the current status of the development of high-performing laser pumped vapor cell frequency standards. The more recent approaches have been highlighted, as well as the best results reached in terms of frequency stability.

The state selection performed via intensity optical pumping is more efficient when performed by a laser instead of a lamp. However, the laser induces a strong coupling between optical and microwave coherences, so that laser fluctuations are transferred to the clock transition through different mechanisms. A number of different techniques have been envisaged by several groups in order to mitigate these effects.

For instance, we have seen that in the continuous DR approach, it is possible to conveniently minimize the light-shift coefficients but they still remain relatively large, limiting eventually the clock stability.

CPT provides a first-order cancellation of light-shift because of the symmetry inherent to the Λ scheme. However, light-shift can be compensated in CPT but not fully eliminated and also in this case it may contribute to degrade the medium-term clock stability.

From a physical point of view, we notice that both in DR and in CPT, the atoms

can be regarded as three-level systems where optical and microwave coherences are simultaneously excited, interfering among them. This is also true for pulsed CPT. In fact, despite there is a phase in which the atoms evolve freely, during the Λ pulse the two ground-state levels and the excited state are all involved in the interaction. In addition, in the double Λ technique, not only the laser intensity, but also the polarization affects the clock frequency.

The pulsed operation demonstrated more effective to strongly reduce light-shift. Indeed, in this case the atoms really behave as a two-level system (the two clock levels) while making the clock transition and light-shift only appears in a residual form, provided the optical pumping is performed with a sufficiently high intensity.

The FM-to-AM laser noise conversion, on the other hand, still remains an issue also in the POP technique. The use of a laser with a very narrow linewidth as well as the detection of the clock signal through the magneto-optical rotation can be very helpful to reduce this effect and to approach the fundamental shot-noise limit.

On the other hand, we have seen that not only the laser but also other parameters can play a role to limit the clock stability. One of these is the interrogating microwave. Work is in progress in order to develop ultra low phase noise synthesis chain. The proposed technique of interleaved atomic clocks could be used to relax the requirements for the microwave synthesizer.

Moreover, it is of basic importance to reduce as much as possible the inhomogeneities of the laser and RF fields inside the active atomic medium and the temperature inhomogeneities in the whole cell, especially for not limiting the long term stability.

Taking into account the experimental results achieved until today and the very recent proposals reported in chapter 6, it appears feasible to reach an Allan standard deviation $\sigma_y(\tau) < 1 \times 10^{-13}\tau^{-1/2}$ in the short term, a flicker frequency limit $\sigma_y(\tau) \le 1 \times 10^{-15}$ in the medium term and a drift of the order of $1 \div 2 \times 10^{-15}$/day.

Finally, we have also seen that a vapor cell clock based on cold atoms has been realized. Besides the frequency stability result, this clock is quite remarkable since the absence of buffer gas allows the evaluation of an accuracy budget.

$$* \ * \ *$$

REFERENCES

[1] CAMPARO J., *Phys. Today*, **60** (2007) 33.
[2] KASTLER A., *J. Phys. Radium*, **11** (1950) 255.
[3] BENDER P. L., BEATY E. C. and CHI A. R., *Phys. Rev. Lett.*, **1** (1958) 311.
[4] VANIER J. and AUDOIN C., *The Quantum Physics of Atomic Frequency Standards* edited by ADAM HILGER Bristol, 1989.
[5] DUPUIS R. T., LYNCH T. J. and VACCARO J. R., *Proceedings of the 2008 IEEE International Frequency Control Symposium* edited by JADUSLIWER B. (Honolulu, Hawaii-USA) 2008, pp. 655-660.
[6] WALLER P., GONZALEZ S., BINDA S., SESIA I., HIDALGO I., TOBIAS G. and TAVELLA P., *IEEE Trans. Ultrason. Ferroelct. Freq. Control*, **57** (2010) 738.
[7] *Glonass Navigation Satellite System, interface controcl document, Edition 5.1, Moscow, 2008*

[8] HAN CHUNHAO, CAI ZHIWU, LIN YUTING, LIU LI, XIAO SHENGHONG, ZHU LINGFENG, AND WANG XIANGLEI, *International Journal of Navigation and Observation* Volume 2013, Article ID 371450, http://dx.doi.org/10.1155/2013/371450.

[9] PETREMAND Y, AFFOLDERBACH C., STRAESSLE R., PELLATON M., BRIAND D., MILETI G., and DE ROOIJ N. F., *J. Micromech. Microeng.*, **22** (2012) 025013.

[10] KNAPPE S., *Compr. Microsyst*, **3** (2008) 571.

[11] KITCHING J., KNAPPE S. and HOLLBERG L.,*Appl. Phys. Lett*, **81** (2002) 553.

[12] LUTWAK R., RASHED A., VARGHESE M., TEPOLT G., LEBLANC J., MESCHER M., SERKLAND D. K., GEIB K. M., PEAKE G. M. and AND ROMISCH S., *Proceedings 10th Precise Time and Time Interval Meeting* (Long Beach, CA, USA) 2007, pp. 269-290.

[13] HASEGAWA M., CHUTANI R.K., GORECKI C., BOUDOT R., DZIUBAN P., GIORDANO V., CLATOT S. and MAURI L., *Sensors Actuators A*, **167** (2011) 594.

[14] GONG F., JAU Y.-Y., JENSEN K. and HAPPER W., *Rev. Sci. Instrum.*, **77** (2006) 076101.

[15] LIEW L.-A., KNAPPE S., MORELAND J., ROBINSON H., HOLLBERG L. and KITCHING J., *Appl. Phys. Lett.*, **84** (2004) 2694.

[16] CAMPARO J. C. and FRUEHOLTZ R. P., *J. Appl. Phys.*, **59** (1986) 301; **59** (1986) 3315.

[17] BANDI T., AFFOLDERBACH C., CALOSSO C. E. and MILETI G., *Electron. Lett.*, **47** (2011) 698.

[18] MICALIZIO S., CALOSSO C. E., GODONE A. and LEVI F., *Metrologia*, **49** (2012) 425.

[19] BATTISTI A., COSENTINO A, SAPIA A., GIOIA M., BORELLA A., GODONE A., LEVI F., CALOSSO C., MICALIZIO S., *Proceedings of the European Frequency and Time Forum* (Neuchatel, Switzerland) 2014, to be published.

[20] BELLONI M., BATTISTI A., COSENTINO A., SAPIA A., BORELLA A., MICALIZIO S., GODONE A., LEVI F., CALOSSO C., ZULIANI L., LONGO F., DONATI M.,, *Proceedings of the 41st Annual Precise Time and Time Interval Systems and Applications Meeting* (Santa Ana Pueblo, New Mexico) 2009, pp. 519-530.

[21] DE SARLO L., LANGLOIS M., HOLLEVILLE D., LOURS M., DIMARCQ N., SCHAFF J.-F., BERNON S. and DESRUELLE B., *Proceedings of the European Frequency and Time Forum* (Neuchatel, Switzerland) 2014, to be published.

[22] DICKE R. H., *Phys. Rev.*, **89** (1953) 472.

[23] GODONE A., LEVI F., MICALIZIO S. and VANIER J., *Phys. Rev A*, **62** (2000) 053402.

[24] GODONE A., LEVI F. and MICALIZIO S., *Coherent Population Trapping Maser* edited by CLUT EDITRICE (Torino, 2002).

[25] VANIER J. and MANDACHE C., *Appl. Phys. B*, **87** (2007) 565.

[26] MICALIZIO S., GODONE A., LEVI F. and CALOSSO C., *Phys. Rev. A*, **79** (2009) 013403.

[27] VANIER J., SIMARD J. F. and BOULANGER J. S., *Phys. Rev. A*, **9** (1974) 1031.

[28] VANIER J., KUNSKI R., BRISSON A. and PAULIN P., *J. Phys. Colloques*, **42 (C8)** (1981) 139.

[29] BANDI T, AFFOLDERBACH C. and MILETI G., *J. App. Phys.*, **111** (2012) 124906.

[30] DEMTROEDER, *Laser Spectroscopy, Basic Concepts and Instrumentation* edited by SPRINGER, 3RD EDITION (Berlin, Germany) 2002.

[31] SABURI Y., KOGA Y., KINUGAWA S., IMAMURA T., SUGA H. and OHUCHI Y., *IEEE Electron. Lett.*, **30** (1994) 633.

[32] CAMPARO J. COFFER J. and TOWNSEND J., *J. Opt. Soc. Am. B*, **22** (2005) 529.

[33] MILETI G., DENG J., WALLS F. L., JENNINGS D. A. and DRULLINGER R. E., *IEEE J. Quantum Electron.*, **34** (1998) 233.

[34] KRAMER G., *Proceedings of the Conference on Precision Electromagnetic Measurements* (London, UK) 1974, p. 157.

[35] BANDI T., PELLATON M., MILETIC D., AFFOLDERBACH C., GRUET F., MATTHEY R., MILETI G., STEFANUCCI C., VIOLETTI M., MERLI F., ZURCHER J. and SKRIVERVIK A.K., *Proceedings of the IEEE International Frequency Control Symposium (FCS)* (Baltimore, MD, USA) 2012, pp. 1 - 6.

[36] BANDI T., *PhD thesis* UNIVERSITE DE NEUCHATEL 2013.

[37] Bandi T., Affolderbach C., Mileti G., Stefanucci C., Merli F., Skrivervik A.K., Calosso C.E., *Proceedings of the European Frequency and Time Forum (EFTF)* (Goteborg, Sweeden) 2012, pp. 494-496.

[38] Stefanucci C., Bandi T., Merli F., Pellaton M., Affolderbach C., Mileti G. and Skrivervik A. K., *Rev. Scien. Instrum.*, **83** (2012) 104706.

[39] Calosso C. E., Micalizio S., Godone A., Bertacco E.K. and Levi F., *IEEE Trans. Ultrason. Ferroelect. Freq. Control*, **54** (2007) 1731.

[40] Davidovits P. and Novick R., *Proceedings of the IEEE*, **54** (1966) 155.

[41] Vanier J., *Phys. Rev.*, **168** (1968) 129.

[42] Michaud A., Tremblay P. and Tetu M., *IEEE Trans. Instrum. Meas.*, **40** (1991) 170.

[43] Deng J., Liu J., An S., Tan Y. and Zhu X., *IEEE Trans. Instrum. Meas.*, **43** (1994) 549.

[44] Oura N. Kuramochi N., Domon W., Komiyama T. and Shirato R., *Proceedings of the European Frequency and Time Forum (EFTF)* (Noordwijk, The Netherland) 1992, pp. 527-530.

[45] Tetu M., Brousseau R. and Vanier J.,*IEEE Trans. Instrum. Meas.*, **29** (1980) 94.

[46] Tetu M., Tremblay P., Lesage P. and Petit P.,*IEEE Trans. Instrum. Meas.*, **32** (1983) 410.

[47] Tetu M., Brousseau R, Cyr N., Michaud A., Tremblay P. and Villeneuve B., *Proceedings of the Frequency Control Symposium (FCS)* (Philadelphia, Pennsylvania, US) 1985, pp. 64-71.

[48] Tetu M., Busca G. and Vanier J.,*IEEE Trans. Instrum. Meas.*, **22** (1973) 250.

[49] Busca G., Brousseau R. and Vanier J.,*IEEE Trans. Instrum. Meas.*, **24** (1975) 291.

[50] Cohen-Tannoudji and Barrat J. P., *J. Phys. (Paris)*, **22** (1961) 329; **22** (1961) 443.

[51] Mathur B. S., Tang H. and Happer W., *Phys. Rev.*, **171** (1968) 11.

[52] Camparo J. Coffer J. and Townsend J., *Proceedings of the IEEE International Frequency Control Symposium* (Montreal Canada) 2004, pp. 134-136.

[53] Affolderbach C., Droz F. and Mileti G., *IEEE Trans. Instrum. Meas.*, **55** (2006) 429.

[54] Bandi T., Affolderbach C., Mileti G., Stefanucci C., Merli F. and Skrivervik A.K., *Proceedings of European Frequency and Time Forum and International Frequency Control Symposium (EFTF/IFC) Joint* ((Prague, Czech Republic) 2013 pp. 220-223.

[55] Micalizio S., Godone A., Calosso C., Levi F., Affolderbach C. and Gruet F., *IEEE Trans. Ultrason. Ferroelect. Freq. Control*, **59** (2012) 457.

[56] Camparo J.C., Buell W.F., *Proceedings of the 1997 IEEE International Frequency Control Symposium* (Orlando, FL, USA) 1997 pp. 253-258.

[57] Camparo J.C., *IEEE International Frequency Control Symposium* (New Orleans, LA, USA) 2002, pp. 476-479.

[58] Camparo J.C., Coffer J.G. and Townsend J.J., *Proceedings of the 2004 IEEE International Frequency Control Symposium and Exposition, 2004. , 2004, 134-136*;

[59] Arimondo E., *Prog. Opt.*, **XXXV** (1996) 257.

[60] Vanier J., *Appl. Phys. B*, **81** (2005) 421.

[61] Shah V. and Kitching J., *Advances At. Mol. Opt. Phys.*, **59** (2010) 21.

[62] Alzetta G., Gozzini A., Moi L. and Orriols G., *Nuovo Cimento*, **B 36** (1976) 5.

[63] Thomas J. E., Hemmer P. R., Ezekiel S., Leiby, Jr. C. C., Picard R. H. and Willis C. R., *Phys Rev. Lett.*, **48** (1982) 867.

[64] Ezekiel S. et al., *Phys. Rev. Lett.*, **50** (1983) 549.

[65] Hemmer P. R., *J. Opt. Soc. Am. B*, **10** (1993) 1326.

[66] Cyr N., Tetu M. and Breton M., *IEEE Trans. Instrum. Meas.*, **42** (1993) 640.

[67] Vanier J., Godone A. and Levi F., *Phys Rev A*, **58** (1998) 2345.

[68] Levi F., Godone A., Vanier J., Micalizio S. and Modugno G., *Eur. Phys. J. D*, **12** (2000) 53.

[69] Godone A., Levi F. and Micalizio S., *Phys. Rev. A* , **65** (2002) 033802.

[70] Levi F., Godone A. and Vanier J., *IEEE Trans. UFFC* , **47** (2000) 466.

[71] Zhu M. and Cutler L., *Proceedings 32 PTTI, 2000, 311*

[72] Godone A., Levi F., Micalizio S. and Calosso C., *Phys. Rev. A*, **70** (2004) 012508.

[73] Godone A., Levi F., Micalizio S. and Vanier J., *Eur. Phys. J. D*, **18** (2002) 5.

[74] Nagel A. Affolderbach C., Knappe S., Wynands R., *Phys. Rev. A*, **61** (2000) 012504.

[75] Stahler M., Wynands R., Knappe S., Kitching J., Hollberg L., Taichenachev A. et al., *Opt. Lett.*, **27** (2002) 1472.

[76] Jau Y.-Y., Miron E., Post A. B., Kuzma N. N. and Happer W, *Phys. Rev. Lett*, **93** (2004) 160802.

[77] Taichenachev V. et al, *JETP Letters*, **80** (2004) 236.

[78] Kazakov G., Mazets I., Rozhddestvensky Y., Milet G., Delporte J. and Matisov B., *Eur. Phys. J. D*, **35** (2005) 445.

[79] Taichenachev A. V., Yudin V. I., Velichansky V. L. and Zibrov S. A., *JETP Letters*, **82** (2005) 398.

[80] Taichenachev V. A., Tumaikin A. M., Yudin V. I., Stahler M. ,Wynands R., Kitching J. and Hollberg L., *Phys. Rev. A*, **69** (2004) 024501

[81] Merimaa M., Lindvall T., Tittonen I. and Ikonen E., *J. Opt. Soc. Am. B*, **20** (2003) 273.

[82] Vanier J. et al., *IEEE trans. Instrum Meas*, **54** (2005) 2531

[83] Knappe S., Wynands R., Kitching J., Robinson H. and Hollberg L., *J. Opt. Soc. Am. B*, **18** (2001) 1545.

[84] Kitching J., Knappe S., Vukicevic M., Hollberg L., Wynands R. and Weidmann W., *IEEE Trans. Instrum. Meas.*, **49** (2000) 1313.

[85] Zhu M., *Proceedings of the Joint Meeting 17th European Frequency and Time Forum and 2003 IEEE International Frequency Control Symposium* (Tampa, FL, USA) 2003, pp. 16-21.

[86] Zanon T., Guerandel S., de Clercq E., Holleville D, Dimarcq N. and Clairon A., *Phys. Rev. Lett.*, **94** (2005) 193002.

[87] Liu X., Merolla J.-M., Guerandel S., Gorecki C., de Clercq E. and Boudot R., *Phys. Rev. A* , **87** (2013) 013416.

[88] Godone A. and Micalizio S., *unpublished.*

[89] Liu X., Merolla J.-M., Guerandel S., Gorecki C., de Clercq E. and Boudot R., *Opt. Express*, **21** (2013) 12451.

[90] Kozlova O., Danet J.-M., Guerandel S. and de Clercq E., *IEEE Transactions on Instrum. Meas.*, **63** (2014) 1863.

[91] Guerandel S., Zanon T., Castagna N., Dashes F., de Clercq E., Dimarcq N. and Clairon A., *IEEE Trans. Instrum. Meas.*, **56** (2007) 383.

[92] Castagna N., Boudot R., Guerandel S., de Clercq E., Dimarcq N. and Clairon A., *IEEE Trans. Ultrason. Ferroelect. Freq. Control*, **56** (2009) 246.

[93] Boudot R., Guerandel S., De Clercq E., Dimarcq N. and Clairon A., *IEEE Trans. Instrum. Meas.*, **58** (2009) 1217.

[94] Godone A., Micalizio S. and Levi F., *Phys. Rev. A*, **70** (2004) 023409.

[95] Alley C. O., *Quantum Electronics* edited by C. H. Townes Editor, Columbia University Press (New York, USA) 1960.

[96] Arditi M. and Carver T. R., *IEEE Trans. Instrum. Meas.*, **13** (1964) 146 .

[97] Godone A., Micalizio S., Levi F. and Calosso C., *Phys. Rev. A*, **74** (2006) 043401.

[98] Micalizio S., Calosso C. E., Levi F. and Godone A., *Phys. Rev. A*, **88** (2013) 033401.

[99] Kang S., Affolderbach C., Gruet F., Calosso C. E. and Mileti G., *Proceedings of the European Frequency and Time Forum* (Neuchatel, Switzerland) 2014, to be published.

[100] English T. C., Jechart E. and Kwon T. M., *Proceedings 10th Precise Time and Time Interval Forum*, ((G) reenbelt, MD, USA) 1978, pp. 147-165.

[101] Lin J., Deng J., Ma Y., He H. and Wang Y., *Opt. Lett.*, **37** (2012) 5036.

[102] Santarelli G., Audoin C., Makdissi A., Laurent P., Dick G. J. and Clairon A., *IEEE Trans. Ultrason. Ferroelct. Freq. Control*, **45** (1998) 887.

[103] Greenhall C., *IEEE. Trans. Ultrason., Ferroelect., Freq. Contr.*, **45** (1998) 895.

[104] Joyet A., Mileti G., Dudle G. and Thomann P., *IEEE Trans. Instrum. Meas.*, **50** (2001) 150.

[105] Francois B., Calosso C. E., Danet J. M. and Boudot R., *Rev. Sci. Instrum.*, **85** (2014) 094709.

[106] Biedermann G. W., Takase K., Wu X., Deslauriers L., Roy S. and Kasevich M. A., *Phys. Rev. Lett.*, **111** (2013) 170802.

[107] Micalizio S., Godone A., Levi F. and Vanier J., *Phys. Rev. A* , **73** (2006) 033414.

[108] Micalizio S., Godone A., Levi F. and Calosso C., *IEEE Trans. Ultrason. Ferroelct. Freq. Control*, **57** (2010) 1524.

[109] Calosso C. E., Godone A., Levi F. and Micalizio S., *IEEE Trans. Ultrason. Ferroelct. Freq. Control*, **59** (2012) 2646.

[110] Bandi T., Affolderbach C., Stefanucci C., Merli F., Skrivervik A. K. and Mileti G., *IEEE Trans. Ultrason. Ferroelct. Freq. Control*, **61** (2014) 1769.

[111] Godone A., Micalizio S., Levi F. and Calosso C., *Rev. Sci. Instrum.*, **82** (2011) 074703.

[112] Einstein A., *Physik. Zeitschr.*, **XVIII** (1917) 121.

[113] Hansch T W. and Schawlow A. L., *Optics Comm.*, **13** (1975) 68.

[114] Ketterle W., Martin A., Joffe A. M. and Pritchard D. E., *Phys. Rev. Lett.*, **69** (1992) 2483.

[115] Guillot E., Pottie P.-E. and Dimarcq N., *Opt. Lett.*, **26** (2001) 1639.

[116] Esnault F.-X., Holleville D., Rossetto N., Guerandel S. and Dimarcq N., *Phys. Rev. A*, **82** (2010) 033436.

[117] Wang Y. Z., *Proceedings of the National Symposium on Frequency Standards* (Chengdu, China) 1979.

[118] D. G. Enzer and W. M. Klipstein, *IEEE Trans. Ultrason. Ferroelct. Freq. Control*, **53** (2006) 1564.

[119] F. Levi, D. Calonico, C. E. Calosso, A. Godone, S. Micalizio, and G. A. Costanzo, *Metrologia*, **51** (2014) 270.